

Advanced Physico-Chemical Modeling of Lithium Plating in Lithium-Ion Batteries

For application in electric vehicles and fast charging at low temperature

Master's thesis in Applied Physics

ANGELICA FORS

SIMON NILSSON

MASTER'S THESIS 2018

Advanced Physico-Chemical Modeling of Lithium-Ion Batteries

For applications in electric vehicles and fast charging at low
temperature

ANGELICA FORS
SIMON NILSSON



CHALMERS
UNIVERSITY OF TECHNOLOGY

Department of Physics
Division of Condensed Matter Physics
CHALMERS UNIVERSITY OF TECHNOLOGY
Gothenburg, Sweden 2018

Advanced Physico-Chemical Modeling of Lithium-Ion Batteries
For applications in electric vehicles and fast charging at low temperature
ANGELICA FORS
SIMON NILSSON

© ANGELICA FORS, 2018.

© SIMON NILSSON, 2018.

Supervisor: Christian Fleischer, Volvo Cars Corporation
Examiner: Patrik Johansson, Department of Physics

Master's Thesis 2018
Department of Physics
Division of Condensed Matter Physics
Chalmers University of Technology
SE-412 96 Gothenburg
Telephone +46 31 772 1000

Cover: Schematic representation of the film layers that form around an active material sphere in the negative electrode

Typeset in L^AT_EX
Gothenburg, Sweden 2018

Advanced Physico-Chemical Modeling of Lithium-Ion Batteries
For applications in electric vehicles and fast charging at low temperature
ANGELICA FORS
SIMON NILSSON
Department of Physics
Chalmers University of Technology

Abstract

The transport sector is responsible for about 14 % of the global greenhouse gas emissions. To make the transition to sustainable transportation it is important to find sustainable alternatives that can compete with today's petrol and diesel vehicles. The most promising alternative is electricity stored in lithium-ion batteries (LIBs) in hybrid electric vehicles (HEVs) and electric vehicles (EVs).

Two challenges that need to be solved to fully compete with petrol and diesel cars are the charging time of LIBs and the service life of EVs and HEVs, where LIBs typically are the limitation due to ageing phenomena. One ageing phenomenon that is problematic in both of these challenges is lithium metal deposition (or lithium plating).

To predict lithium plating accurately complex physics-based models are needed. If accurate enough such models could be used to predict optimal charging conditions to enable for faster battery charging, at low temperatures without damaging the battery. In this project a physics-based model to predict lithium plating in LIBs and fast charging at low temperature has been developed in Simulink.

The model has been validated by comparison with results from models found in literature with very good agreement. A sensitivity analysis of the parameters pointed out the most important parameters for the simulations to be parameters in the negative electrode as well as the diffusion coefficient and the ionic conductivity in the electrolyte. To make accurate simulations at low temperatures an Arrhenius dependence is introduced on relevant material parameters. Even though the results are promising the model validation is mostly done versus existing models. In order to use this model to improve charging routines for LIBs in HEVs and EVs it is necessary to collect data on lithium plating and determine material parameters experimentally.

Keywords: Lithium plating, physics-based modeling, lithium-ion battery, automotive, sustainable future, electric vehicle.

Acknowledgements

We would like to thank our supervisor Christian Fleischer and Volvo Cars Corporation for the opportunity of doing this master thesis. We would also like to thank Christian Fleischer, Kristian Frenander and Johan Scheers at VCC and Evelina Wikner and our examiner Patrik Johansson at Chalmers for their time and clever advice.

The master's thesis project is just half a year out of five years of continuous learning experiences. Therefore we would also like to direct a special thank you to the ones who have made these years a blast! Firstly, to CSN for financial support and hopefully low interest rates in the coming years. Secondly, to all of our fellow heroes for all of your support, you made these years the best.

Angelica Fors and Simon Nilsson, Gothenburg, June 2018

Contents

List of Figures	x
List of Tables	xi
List of Acronyms and Symbols	xiii
1 Introduction	1
1.1 Aim of Project	2
1.2 Project Deliverables	2
1.3 Limitations	2
1.4 Societal, Ethical and Ecological Aspects	3
2 The Lithium-ion Battery	5
2.1 Fundamentals of Batteries	5
2.2 The Lithium-ion Battery	6
2.3 Ageing Phenomena	9
3 Modeling Lithium-ion Batteries	11
3.1 The Newman Model	11
3.2 Modeling of Lithium Plating	18
4 Method	21
4.1 Model Dimensions	21
4.2 The Electric Circuit Network	22
4.3 Temperature Dependence	25
4.4 Calculation procedure	27
5 Validation of Model	29
5.1 Comparison with Arora et al.	29
5.2 Comparison with Tippmann et al.	33
6 Discussion	39
7 Further Work	41

List of Figures

2.1	A schematic drawing of a battery cell during discharge (a) and charging (b).	6
2.2	Comparison of energy density in common secondary battery systems.	7
2.3	The intercalation process. Li-ions intercalate into the negative electrode upon charging and into the positive electrode during discharge.	8
2.4	Comparison of positive (left) and negative (right) electrode materials.	9
2.5	A schematic figure over the different ageing phenomena that occur in LIBs. This figure is reproduced with the permission and courtesy of Jens Groot [1].	10
3.1	A schematic figure of a battery cell. The complex structure in the two electrodes consist of binder and conducting additives (black), active material (grey) and electrolyte (blue).	12
3.2	A schematic figure illustrating the film surrounding the active material particle.	20
4.1	The discretization of the cell. The blue domain represents the separator with the positive electrode to its left and the negative electrode to the right.	22
4.2	The discretization of the active material spheres.	22
4.3	A schematic drawing of the electric circuit network.	23
4.4	A schematic picture over the calculation procedure in the model.	27
5.1	Thickness of the deposited lithium-film as a function of time for different charging currents and excess capacities in the negative electrode.	31
5.2	A sensitivity analysis of the material parameters used in the comparison with Arora et al.	32
5.3	A sensitivity analysis of the material parameters used in the comparison with Arora et al.	33
5.4	The anode potential for charging currents between 0.1C–1C at 0°C and 4.2V as cut-off voltage.	36
5.5	The onset of lithium plating as a function of charging current and temperature with 4.2V as cut-off voltage.	36
5.6	The onset of lithium plating as a function of SOC and charging current at –15°C and with 4.2V as cut-off voltage.	37

5.7	A sensitivity analysis of the material parameters used in the comparison with Tippmann et al.	38
-----	---	----

List of Tables

5.1	Parameters used in the comparison with Arora et al.	30
5.2	Parameters used in the comparison with Tippmann et al.	34
5.3	Temperature dependent parameters used in the comparison with Tippmann et al.	35

List of Symbols and Acronyms

Symbols

A	Cross-section area, m^2	U_1	Open-circuit potential, V
A_i	Electrode surface area, m^2	v	Velocity, m/s
a	Specific interfacial area, m^2/m^3	x	Distance from positive electrode, m
<i>brug</i>	Bruggeman factor	z	Charge number
c	Concentration, mol/m^3	α	Transfer coefficient
c_τ	Maximum theoretical concentration, mol/m^3	δ	Length of cell component, m
D	Diffusion coefficient, m^2/s	ε	Volume fraction
\mathcal{D}	Diffusion coefficient as a function of electrochemical potential, m^2/s	η	Overpotential, V
E_{act}	Activation energy, J/mol	κ	Ionic conductivity, S/m
F	Faraday constant, C/mol	μ	Electrochemical potential, J/mol
f_\pm	Mean molar activity coefficient	ν	Dimensionless exchange current
I	Superficial current density, A/m^2	ν_+, ν_-	Number of ions into which a mole of electrolyte dissociates
i	Current density, A/m^2	ρ	Density, kg/m^3
i_0	Exchange current density, A/m^2	σ	Electric conductivity, S/m
j_n	Pore wall flux, mol/m^2s	ψ_i	Dimensionless concentration in electrode i
$K_{i,j}$	Interaction coefficient, J_s/m^5		
k	Reaction rate constant, $m^{5/2}/mol^{1/2}s$		
M	Molar mass, g/mol		
N	Net molar flux, mol/m^2s		
R	Gas constant, $J/molK$		
R_s	Radius of active material spheres, m		
r	Distance in active material spheres, m		
T	Temperature, K		
T_{ref}	Reference temperature, K		
t	Time, s		
t_i^0	Transference number of specie i		

Subscripts

$+$, $-$	Cation, Anion
0	Solvent
$1, 2$	Solid phase, liquid phase
a	Active material
a, c	Anodic, Cathodic
<i>eff</i>	Effective value
i, j	Specie
<i>Li</i>	Lithium plating
n, p	Negative-, positive electrode
T	Total
s	Surface

Acronyms

CC	Constant current
CTL	Charge transfer limitation
CV	Constant voltage
EV	Electric vehicle
GHG	Greenhouse gas
HEV	Hybrid electric vehicle
LIB	Lithium-ion battery
Li-ion	Lithium-ion
LMO	Electrode of LiMn_2O_4
NCA	Electrode of $\text{LiNi}_x\text{Co}_y\text{Al}_z\text{O}_2$
NMC	Electrode of $\text{LiNi}_x\text{Mn}_y\text{Co}_z\text{O}_2$
OCP	Open-circuit potential
redox	Reduction-oxidation
SDL	Solid diffusion limitation
SEI	Solid electrolyte interphase
SOC	State-of-charge
SOH	State-of-health
VCC	Volvo cars corporation

1

Introduction

The transport sector is responsible for 14 % of the global greenhouse gas (GHG) emissions and more than 50% of these emissions originates from the combustion of petroleum-based products in combustion engines of cars and light-duty trucks [2]. To reduce the GHG emissions from the transport sector sustainable alternatives are needed. The most promising alternative is electricity stored in lithium-ion batteries (LIBs). In the Fall of 2017 Volvo Cars Corporation (VCC) announced that they only will develop hybrid electric vehicles (HEVs) and electric vehicles (EVs) from 2019 and onwards [3].

However, there are still challenges of LIBs. Today the service life for EVs and HEVs are expected to be 10 years and 15 years, respectively [4, 5]. LIBs are typically the limitation due to ageing phenomena which result in reduced storage capacity and power. Another problem that LIBs struggle with is the charging time. In order to compete with today's petrol and diesel cars it is desirable to have a charging time comparable with the fuelling time of those cars [6].

Different phenomenon contributes to ageing of LIBs. One phenomena is lithium metal deposition (or lithium plating). Lithium plating means that lithium metal is deposited on the anode and will happen when the intercalation of lithium in the anode is hindered, either by a slow charge transfer process or slow diffusion of lithium in the active material, which causes the potential of the anode to drop below the potential of Li/Li^+ . The deposited lithium causes a loss in capacity, higher internal resistance in the battery and form dendrites, which potentially could short-circuit the cell and cause a thermal runaway. The phenomenon is known to occur when charging at low temperatures, at high current (fast charging) and at high state-of-charge (SOC) [7, 8]. Since lithium plating occurs if the battery is charged too quickly the phenomenon will also limit the speed at which the battery can be charged, especially at low temperatures.

Ageing phenomena are hard to predict accurately. To understand the underlying ageing phenomenon and ultimately alter the operating conditions complex physics-based models are needed. A physics-based model to model battery performance has been provided to this project. However, this model does not include any ageing phenomena. By using the model as a basis, it can be improved to also include

lithium plating. If accurate enough, this improved model can be used to predict optimal charging conditions for VCC's cars in order to enable for faster battery charging, at low temperatures without damaging the battery.

1.1 Aim of Project

The aim of this thesis work is to create a model for lithium plating in lithium-ion batteries which can be used to predict optimal charging conditions for fast charging at low temperatures.

1.2 Project Deliverables

The deliverables of the project are:

- A physics based model for lithium plating.
- A comparison between the developed model and experimental results, from literature and/or provided by VCC.

1.3 Limitations

There are a variety of ageing phenomena, here the focus is on modeling lithium plating.

Lithium plating is known to happen during high current charging, at low temperature and/or high SOC. However, there are also other physical processes known to cause lithium plating. Since modeling of those processes would require additional physical processes to be added to the model and since lithium plating as a result of the conditions mentioned above is a higher priority issue, this project will be limited to modeling lithium plating as a result of the conditions mentioned above.

Battery cell models are generally ordered as empirical, semi-empirical or completely physics based models [5]. This project will develop a physics based model since these models as such are more accurate and also gives a better understanding of the underlying phenomena of ageing. There are some different physics based models, but since the existing performance model is based on the Newman model, the model developed in the scope of this project will be limited to the Newman model as a basis.

1.4 Societal, Ethical and Ecological Aspects

The transport sector is responsible for 14 % of the global GHG emissions and sustainable alternatives that can compete with today's petrol and diesel vehicles are needed to make the transition to sustainable transportation [2, 6]. This project aims to make EVs and HEVs more competitive by increasing service life and also reducing the charging time of LIBs, which is a contribution to the electrification of vehicles and a contribution in an ecological aspect.

Even though EVs are seen by many as the future of transportation, LIBs have been heavily debated. Lithium is a relatively scarce metal (0,0007% of the earth's crust) that are produced primarily in Chile, Argentina, Bolivia, Australia, China and Zimbabwe [9, 10]. The mining operations are associated with high emissions of GHGs and in many countries the mining operations are also associated with bad working conditions and toxicity [10, 11]. However, by modeling lithium plating this ageing phenomena can be avoided and the LIB can be charged more effectively. By increasing the battery lifetime the demand for lithium can be lowered. In that sense this project can be seen as an attempt to contribute in the conversion to green energy.

LIBs are not the perfect solution for energy-storage and a lot of money and effort are invested to find new and better, materials for batteries. However, until a better alternative is found improving LIBs will keep negative effects to a minimum. The knowledge gained from this research may also prove useful for coming technologies. The methods used in this project are entirely computer-based. This approach reduces the resources needed in comparison of doing a lot of experimental testing, which makes the computer-based approach preferable from an ecological point of view.

2

The Lithium-ion Battery

This chapter will give a brief introduction to batteries in general, a more detailed description of the working principles of LIBs and an overview of the materials that are commonly used as electrodes and electrolyte in the automotive industry today. The chapter will end with a theoretical background to the different ageing phenomena that are known to happen inside a LIB.

2.1 Fundamentals of Batteries

A battery is defined as a device that can transform chemical energy into electric energy. The chemical energy is stored in active materials and the energy is transformed into electric energy via oxidation-reduction (redox) reactions. There are two types of batteries, primary batteries (for single use) and secondary batteries (rechargeable). In secondary batteries the redox reactions are reversible which allows the batteries to be charged and used multiple times [12, 13].

Even though a battery is often referred to as one device, it could be built up of one to several thousand cells that are connected in series and/or in parallel. The basic battery cell consists of a positive and a negative electrode, a charge carrying material and electrolyte. The positive electrode has a higher redox potential than the negative electrode, meaning that it is more prone to reduction. The electrolyte allows the charge carrying material to flow between the two electrodes. During discharge the difference in reduction potential between the electrodes will cause the charge carrying material to be oxidized at the negative electrode, flow through the electrolyte and be reduced at the positive electrode. This redox reaction causes electrons to flow through the electrical wiring from the negative electrode to the positive electrode, transforming chemical energy into electric energy (figure 2.1a). When charging the cell an external power source is used to overcome the difference in reduction potential and thereby reverse the reaction (figure 2.1b).

The electrode at which the reduction reaction occurs is called the cathode while the electrode at which the oxidation reaction occurs is called the anode. Noteworthy is

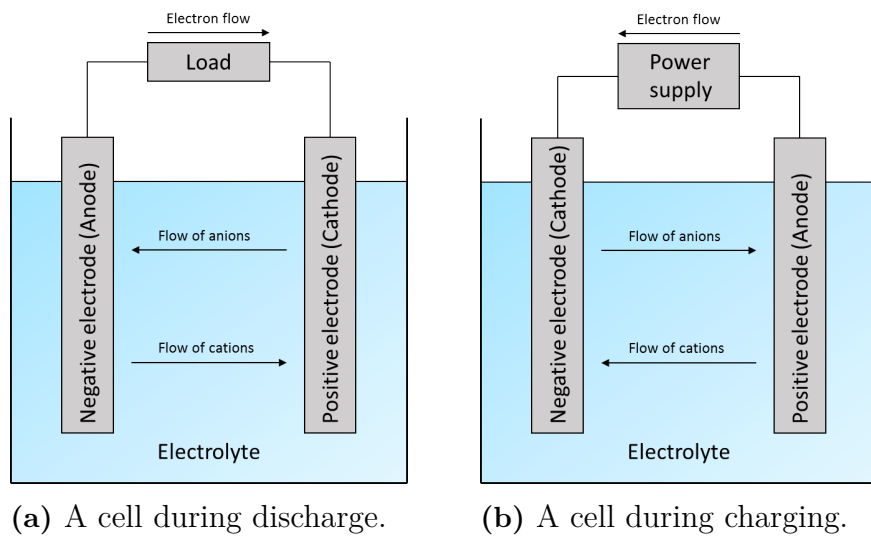


Figure 2.1: A schematic drawing of a battery cell during discharge (a) and charging (b).

that the reduction and oxidation reaction in a secondary battery will occur at different electrodes depending on if the battery is being charged or discharged. Therefore the terms positive and negative electrode will be used in this report to describe the electrodes instead of anode and cathode.

2.2 The Lithium-ion Battery

The first rechargeable battery was the lead-acid battery which was invented in 1859 by Gaston Planté. In 1901 Thomas Edison and Waldemar Jungner invented the Ni-Cd rechargeable battery which was mainly used in heavy duty applications and later for portable applications due to its increased energy density. Since then the battery best suited for portable applications has shifted two times, in 1975 when the metal hybrid (Ni-MH) rechargeable battery was introduced and in 1991 when Sony introduced the first commercial LIB. The LIB has a much higher energy density per volume and also per weight compared to previously known systems (figure 2.2). Since the introduction in 1991 the market share of LIBs has grown rapidly, mainly for portable applications but also for other applications e.g. in the automotive industry [13].

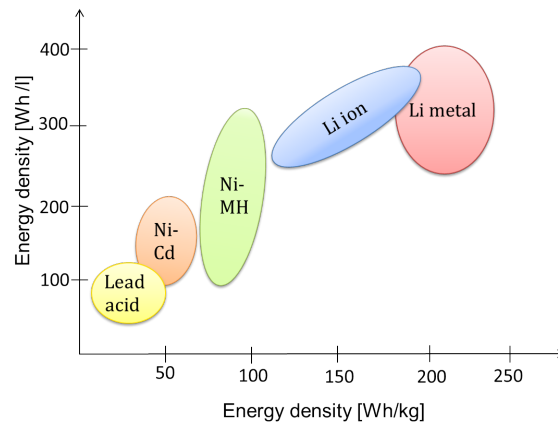


Figure 2.2: Comparison of energy density in common secondary battery systems.

Even though the LIB was commercialized as early as in 1991, there are still a lot of ongoing research on LIBs e.g. to develop new and better electrodes, to better model ageing and to better model state-of-health (SOH). Since modeling of lithium plating in LIBs is the topic of this thesis work, the LIB cell is described in more detail below.

Electrodes

The positive and negative electrode consist of active material, conducting additives and binder. The rechargeable process in a secondary battery is possible due to the intercalation process of lithium-ions (Li-ions) into the active material, meaning that Li-ions are inserted into unoccupied sites in the active material's crystal lattice without affecting the crystal structure notably. In order for the intercalation process to be efficient the electrodes are porous, giving the electrode a large specific surface area and speeding up the intercalation process. The cavities in the porous electrode are filled with electrolyte, allowing the Li-ions to flow to the surface of the active material. During discharge the Li-ions flow through the electrolyte, when the Li-ions reach the surface of the active material in the positive electrode the reduction reaction takes place and the lithium intercalate into the active material. During charging Li-ions are removed from their interstitial sites in the positive electrode, flow through the electrolyte, the Li-ions are reduced at the surface of the active material in the negative electrode and the lithium intercalate into the active material (figure 2.3). The porous structure in the electrode is held together, and attached to the current collectors, by binder.

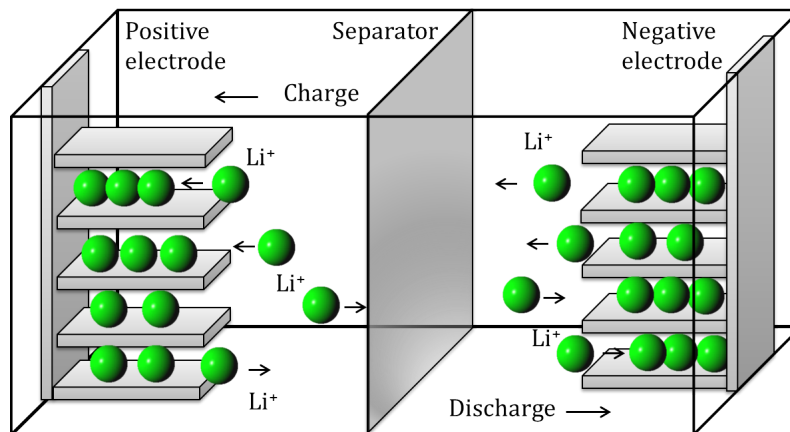


Figure 2.3: The intercalation process. Li-ions intercalate into the negative electrode upon charging and into the positive electrode during discharge.

The materials and the structure of the electrodes determine which properties the electrodes will have. The electrodes should have the following characteristics in order to be efficient [13]:

- A large number of unoccupied sites where lithium could intercalate; in order to achieve high capacity.
- As small changes in the lattice structure as possible caused by intercalation; to get high cycling performance.
- A good electronic and ionic conductivity; to handle charge/discharge with high current density.
- A good chemical stability and not react with the electrolyte.
- Inexpensive, non-toxic and environmentally friendly.
- The positive electrode should have a high potential while the potential of the negative electrode should be low; in order to achieve as high output voltage as possible.

Today, many different materials are used as electrodes, the most common materials are summarized in figure 2.4. In the automotive industry the most common negative electrode material is synthetic and natural graphite due to the low cost of the material, low potential vs. Li/Li^+ and high capacity. The most common positive electrode materials used in the automotive industry today are $\text{LiNi}_x\text{Mn}_y\text{Co}_z\text{O}_2$ (NMC), $\text{LiNi}_x\text{Co}_y\text{Al}_z\text{O}_2$ (NCA) and blend electrodes with either NMC or NCA together with LiMn_2O_4 (LMO) [14]. This is mainly due to the relatively low cost, good stability and high capacities of NMC and NCA while LMO has a high potential, great rate performance and good thermal stability.

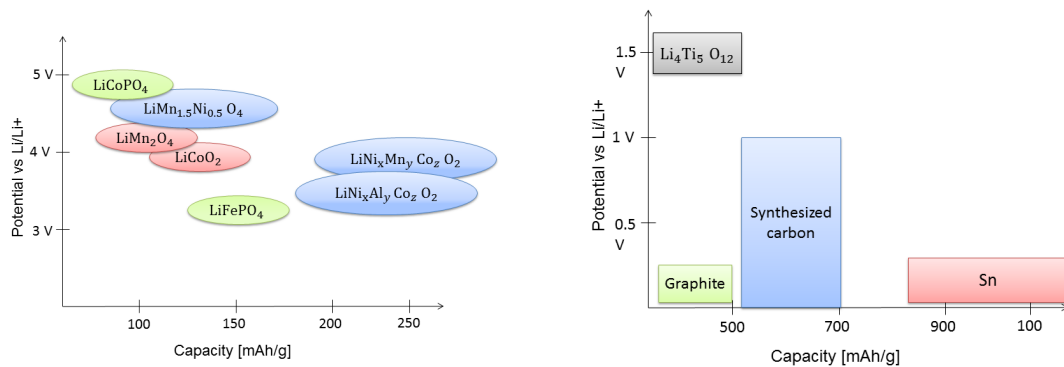


Figure 2.4: Comparison of positive (left) and negative (right) electrode materials.

Electrolyte

The functionality of the electrolyte is to enable flow of lithium-ions between the positive and negative electrode. The electrodes operate outside the electrochemical stability of the electrolyte, which causes the electrolyte closest to the electrodes to decompose during the first charge/discharge cycle. The decomposed electrolyte forms a film around the electrodes called the solid electrolyte interphase (SEI). The SEI has a low electronic conductivity which protects the electrolyte from decomposition and the electrodes from corrosion, but the film is still permeable for Li-ions.

There are different types of electrolytes, such as organic solvent based liquid electrolytes, ionic liquid electrolytes and polymer electrolytes. However, all types contain a lithium salt, solvent and additives to improve material properties. A good electrolyte should have the following characteristics [13]:

- A high ionic and a low electronic conductivity.
- Stable under temperature variations, high voltage and battery reactions.
- Inexpensive, non-toxic and environmentally friendly.

2.3 Ageing Phenomena

Many who have used a laptop or other portable devices with a LIB have experienced that the battery loses capacity over time. This capacity loss is due to the different ageing phenomena that occur in a LIB during use, charging and at rest. The different ageing phenomena that are known to occur in a LIB are for instance SEI growth, lithium plating, corrosion of the current collectors and cracking (figure 2.5). These phenomena lead to a loss of available lithium and therefore a loss of capacity in the battery and also to a raise of impedance in the battery [5].

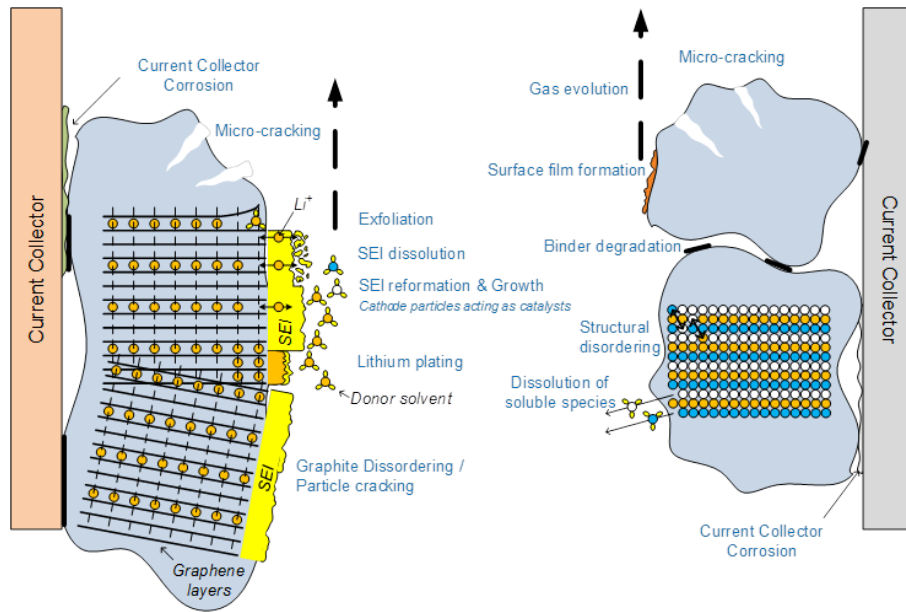


Figure 2.5: A schematic figure over the different ageing phenomena that occur in LIBs. This figure is reproduced with the permission and courtesy of Jens Groot [1].

The ageing phenomenon of interest in this report is lithium-plating, meaning lithium deposits on the surface of the negative electrode. This results in a loss of available lithium and a rise in impedance. The deposited lithium also forms dendrites that, in a worst case scenario, could short circuit the battery cell and cause a thermal runaway.

Lithium plating occur in a LIB since the reduction potential of the preferred intercalation process is slightly above the reduction potential of lithium plating (Li/Li^+). If the intercalation process is hindered the reduction potential of intercalation may fall below that of lithium plating, meaning that this unwanted reaction is energetically favourable. There are two limitations which may cause this drop in the reduction potential, namely the charge transfer limitation (CTL) and the solid diffusion limitation (SDL) [15]. The CTL means that Li-ions accumulate at the electrode interface since electrons are hindered to reach the Li-ions at a fast enough pace, while the SDL means that the diffusion of lithium in the negative electrode is too slow to intercalate the lithium fast enough.

Lithium plating is known to occur when charging at high current, at low temperature and at a high SOC. High current increase the demand of both a fast charge transfer process and a fast diffusion of lithium in the electrodes. At low temperatures, slower molecular dynamics and reaction kinetics makes both CTL and SDL more likely than at room temperature. The SDL is more likely to be rate-limiting at high SOC since the high concentration of already intercalated lithium slows the diffusion of lithium into the electrode [15].

3

Modeling Lithium-ion Batteries

As discussed above, many who have used a portable device with a LIB has experienced capacity loss due to ageing phenomena. Even though the loss of capacity in a cell phone is annoying the short innovation cycles of such devices has made it unnecessary to invest resources in order to avoid battery ageing. However, EV's and HEV's are expected to have a lifetime of at least 10 and 15 years, respectively [4, 5]. Because of this increasing interest in LIBs for long term applications the interest in accurately modeling battery ageing has grown.

Today there are several different approaches to model battery performance without including any ageing phenomena. These approaches range from full empirical models, e.g. artificial neural network models, and semi empirical models, e.g. equivalent circuit models, to physic based models. As may be expected, a physics based model is built on modeling the physical phenomena inside the battery. One advantage with the physics based performance models are that different ageing phenomena easily could be included by adding equations describing the physical phenomena [5].

The developed model in this project is based on the model of Doyle et al. [16] and Arora et al. [17]. Below these models are presented. The implementation of this model is described in detail in Method.

3.1 The Newman Model

In 1993 Doyle et al. published a battery performance model which models the charge/discharge behaviour of a battery cell [16]. Below the structure used in the model and the mathematical expressions used for each part of the cell are explained.

Structure

The LIB consist of a positive electrode, a negative electrode and a separator (figure 3.1). The electrodes are porous, in order to make the intercalation process more efficient, and are usually made of active material, conducting additives and binder. The voids in these porous structures are filled with electrolyte. The complex structure in the electrodes makes microscopic modeling of the electrodes impossible. Because of this the Newman model is based on porous electrode theory, which treats the electrode as a superimposed continua meaning that all materials in the electrode are represented in each point in the electrode by a volume fraction ϵ [18, 19]. With this approach the complex structure can be expressed in macroscopic terms and as a one dimensional problem.

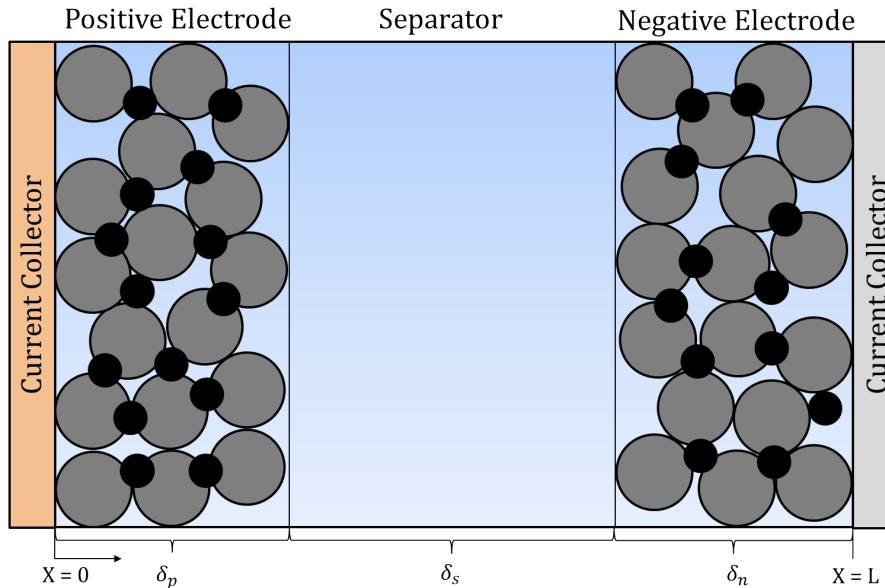


Figure 3.1: A schematic figure of a battery cell. The complex structure in the two electrodes consist of binder and conducting additives (black), active material (grey) and electrolyte (blue).

Even though the macroscopic approach allows the system to be described as a one dimensional problem, the Newman model is pseudo two dimensional. The second dimension comes from that the diffusion process of intercalated lithium in the electrodes are described as diffusion in the spheres of active material.

Mathematical Description of the Separator

When voltage is applied in a LIB there will be a difference in electrochemical potential over the separator. This will cause the Li-ions to move from high to low

electrochemical potential, leading to a concentration gradient. The concentration gradient is counteracted by diffusion. In this section these two driving forces are described mathematically by a material balance which could be used to calculate the concentration in the separator. The Li-ions experience a resistances when moving in the separator. These resistances are accounted for by a mathematical expression describing how the potential varies depending on position in the separator.

Defining the Material Balance in the Separator

A general material balance for mass transport of specie i is defined in equation 3.1 below.

$$\underbrace{\frac{\partial c_i}{\partial t}}_{\text{accumulation}} = \underbrace{\nabla N_i}_{\text{net molar flux}} + \underbrace{P_i}_{\text{production}} \quad (3.1)$$

Here c is the concentration, t is the time, N is the net molar flux and P represent the production from chemical reactions.

Since no chemical reactions take place in the separator (at least not considered in this derivation) the production term in equation 3.1 could be set to 0. To find an expression for the net molar flux the electrolyte is treated as a concentrated solution. In such a solution the driving force is the difference in electrochemical potential, $c_i \nabla \mu_i$, described by equation 3.2.

$$c_i \nabla \mu_i = \sum_{j \neq i} K_{ij} (v_j - v_i) \quad (3.2)$$

Here μ is the electrochemical potential, K_{ij} is the interaction coefficient and describes the interactions between species i and j . $v_j - v_i$ is the difference in velocities between the different species in the electrolyte.

For a solution containing anions (-), cations (+) and solvent (0) equation 3.2 can be written in two different transport equations (equation 3.3 and 3.4).

$$c_+ \nabla \mu_+ = K_{0+} (v_0 - v_+) + K_{-+} (v_- - v_+) \quad (3.3)$$

$$c_- \nabla \mu_- = K_{0-} (v_0 - v_-) + K_{+-} (v_+ - v_-) \quad (3.4)$$

Equation 3.3 and 3.4 needs to be rewritten to equations describing the molar flux as a function of the driving force electrochemical potential. Using that the net molar flux is defined as $N_i = c_i v_i$, that the current density i in the liquid phase (subscript 2) is defined as $i_2 = F \sum_i z_i N_i$ (where F is the Faraday constant and z is the charge number) and that the velocity of the electrolyte can be set to 0, the equations 3.3 and 3.4 yield equation 3.5 and 3.6.

$$N_+ = -\frac{\nu_+ \mathcal{D} c_T}{\nu R T c_0} c \nabla \mu + \frac{i_2 t_+^0}{z_+ F} \quad (3.5)$$

$$N_- = -\frac{\nu_- \mathcal{D} c_T}{\nu R T c_0} c \nabla \mu + \frac{i_2 t_-^0}{z_- F} \quad (3.6)$$

Here \mathcal{D} is the diffusion coefficient expressed in terms of electrochemical potential, t_i^0 is the transference number and describes the fraction of current carried by species i , R is the gas constant, T is the temperature, ν_+ and ν_- is the number of cations and anions into which a mole of electrolyte dissociates and ν is the dimensionless exchange current.

The diffusion coefficient D is usually expressed in terms of the gradient of concentration and not in electrochemical potential as \mathcal{D} . Therefore a correlation between D and \mathcal{D} is needed. This correlation can be described by equation 3.7.

$$\frac{\mathcal{D} c_T}{\nu R T c_0} c \nabla \mu = D \left(1 - \frac{d \ln c_0}{d \ln c} \right) \nabla c \quad (3.7)$$

Inserting equation 3.5 and equation 3.7 in the general material balance described by equation 3.1 the material balance in the separator is described by equation 3.8.

$$\frac{\partial c}{\partial t} = \nabla \cdot \left(D(c) \left(1 - \frac{d(\ln c_0)}{d(\ln c)} \right) \nabla c \right) - \frac{i_2 \cdot \nabla t_+^0(c)}{z_+ \nu_+ F} \quad (3.8)$$

Assuming that the solvent concentration is not a function of the electrolyte concentration and that the transference number t_+^0 does not depend on the concentration equation 3.8 can be reduced to equation 3.9.

$$\frac{\partial c}{\partial t} = \nabla \cdot D(c) \nabla c \quad (3.9)$$

Defining the Variation in Potential in the Separator

To define the variation in potential the current density, i_2 , first need to be defined (equation 3.10). The derivation of the current density is pretty tedious and can be found in literature [19].

$$i_2 = -\kappa(c) \nabla \Phi_2 + \frac{\kappa(c) 2RT}{F} \left(1 + \frac{\partial \ln f_{\pm}}{\partial \ln c} \right) (1 - t_+^0(c)) \nabla \ln c \quad (3.10)$$

Here f_{\pm} is the mean molar activity coefficient and κ is the ionic conductivity of the electrolyte.

The variation in potential in the separator, $\nabla\eta$, is defined by dividing equation 3.10 with the ionic conductivity which results in (equation 3.11).

$$\nabla\eta = -\frac{i_2}{\kappa(c)} + \frac{2RT}{F} \left(1 + \frac{\partial \ln f_{\pm}}{\partial \ln c} \right) (1 - t_+^0(c)) \nabla \ln c \quad (3.11)$$

Boundary Conditions in the Separator

The boundary conditions between the separator and the electrodes ($x = \delta_p$ and $x = \delta_p + \delta_s$ (figure 3.1)) are decided to be continuous. This means that the flux and concentration of each species as well as the potential in the solution phase are continuous.

Mathematical Description of the Electrodes

There are three processes that need to be accounted for in the electrodes; the flow of Li-ions in the electrolyte, the diffusion of lithium in the active material spheres and the electron charge transfer in the Li-ion intercalation reaction occurring at the surface of the active material. Four mathematical expressions are needed to describe the processes in the electrodes. Two of these expressions are material balances which are needed to calculate the concentration in the electrolyte and the active material respectively. The remaining two mathematical expressions describe the charge transfer reaction and how the potential will vary depending on the position in the electrode.

Defining the Material Balance in the Electrolyte

The material balance for the Li-ions in the electrolyte in the porous electrodes is expressed in equation 3.12 below.

$$\varepsilon_2 \frac{\partial c}{\partial t} = \nabla \cdot (D_{eff}(c) \nabla c) + \frac{aj_n(1 - t_+^0)}{\nu_+} \quad (3.12)$$

Here j_n is the pore wall flux. D_{eff} is the effective diffusion coefficient and is explained later in this report (equation 3.13).

As expected the material balance in equation 3.12 is similar to the material balance in the separator (equation 3.9). However, the material balance for the liquid phase in the electrodes also accounts for the pore-wall flux of Li-ions between the electrolyte and the active material by adding a production-term in the equation. Furthermore, the volume fraction of electrolyte and the added path length for Li-ions in the electrolyte in the electrode compared to the free flow in the separator has to be accounted for. This is done by adding the volume fraction to the equation and using the effective diffusion coefficient (equation 3.13). The ionic conductivity (κ)

and the electric conductivity (σ) are also affected by the added path length (equation 3.14 and 3.15) and will be used later when defining the variation in potential in the electrodes.

$$D_{eff} = D\varepsilon^{brug} \quad (3.13)$$

$$\kappa_{eff} = \kappa\varepsilon^{brug} \quad (3.14)$$

$$\sigma_{eff} = \sigma\varepsilon^{brug} \quad (3.15)$$

Here *brug* is the Bruggeman factor and the subscript *eff* denotes that the effective value is used.

The boundary conditions for the material balance in the electrolyte are that the flux of ionic species is equal to zero at the current collector boundary (equation 3.16).

$$N_i = 0 \quad \text{at} \quad x = 0 \quad \text{and} \quad x = L \quad (3.16)$$

Defining the Material Balance in the Active Material

The diffusion of intercalated lithium in the active material is approximated by diffusion in spheres with the radii R_s . The material balance for the active material spheres only needs to include the net flux term caused by diffusion and can be seen below (equation 3.17).

$$\frac{\partial c_a}{\partial t} = D_a \left[\frac{\partial^2 c_a}{\partial r^2} + \frac{2}{r} \frac{\partial c_a}{\partial r} \right] \quad (3.17)$$

Where r is the direction perpendicular to the surface of the sphere.

The boundary conditions for diffusion in the active material can be seen in the equation 3.18 and 3.19 below. The first boundary condition comes from symmetry and the second boundary condition links the pore wall flux and the rate of diffusion at the interface between active material and electrolyte.

$$\frac{\partial c_a}{\partial r} = 0 \quad \text{at} \quad r = 0 \quad (3.18)$$

$$j_n = -D_a \frac{\partial c_a}{\partial r} \quad \text{at} \quad r = R_s \quad (3.19)$$

The Charge Transfer Reaction

The previously described material balances in the electrode and the diffusion in the active material are coupled via the charge transfer reaction. This is described by the Butler-Volmer equation which relates the reaction rate to the surface overpotential (equation 3.20).

$$I = i_0 \left[\exp\left(\frac{\alpha_a F}{RT} \eta_s\right) - \exp\left(-\frac{\alpha_c F}{RT} \eta_s\right) \right] \quad (3.20)$$

Where i_0 is the exchange current density defined in equation 3.22, η_s is the surface potential defined in equation 3.21 and α is the transfer coefficient. The subscripts s stands for surface, a is for anodic reaction and c is for cathodic reaction.

$$\eta_s = \Phi_1 - \Phi_2 - U_1(c) \quad (3.21)$$

$$i_{0,i} = F k_i (c_{\tau,i} - c_i)^{\alpha_a} c_i^{\alpha_c} c_2^{\alpha_a} \quad (3.22)$$

In the expressions above U_1 is the open-circuit potential (OCP) and k is the reaction rate constant.

The OCP in equation 3.21 will vary as the amount of intercalated lithium changes. This is generally accounted for by fitting a function to experimental data on how the OCP varies as a function of the SOC. Since this fit will vary depending on the active material used in each electrode the equations used for the OCP is presented in the Validation of Model.

Defining the Variation in Potential in the Electrodes

The variation in potential in the electrodes can be found in equation 3.23 below. As may be noted this equation is also similar to the corresponding equation in the separator (equation 3.11). However, since the electrodes consist of both a liquid phase (subscript 2) and a solid phase (subscript 1) an extra term has been added to account for the variation in potential caused by the electric current in the solid phase i_1 , which is described by Ohm's law. The current density in the liquid and solid phase are related via the superficial current density $I = i_1 + i_2$.

$$\nabla \eta = -\frac{i_1}{\sigma_{eff}} + \frac{i_2}{\kappa_{eff}} + \frac{2RT}{F} (1 - t_+^0(c)) \nabla \ln c \quad (3.23)$$

3.2 Modeling of Lithium Plating

In the literature review of this project two different approaches to model lithium plating have been found. The first approach was proposed by Arora et al. in 1999 [17]. The authors suggested that lithium plating would occur when the overpotential for this reaction is negative ($\eta_{Li} < 0$). The second approach to model lithium plating was proposed by Purushothaman et al. in 2006 who suggested that lithium plating would occur when the concentration of Li-ions at the electrode-electrolyte interface reaches a saturation concentration [20].

Only a few attempts to validate the models for lithium plating has been found in the literature review of this project. These attempts were done by Ge et al. who expanded the Arora model to investigate lithium plating at low temperature by including an Arrhenius dependence for relevant variables and by Tippmann et al. who coupled the Arora model to a 0D thermal model [21, 22]. Both these articles show promising results, however the validations are done with few data points. No effort to validate the approach suggested by Purushothaman et al. has been found. Since there have been a lot more work done based on the approach suggested by Arora et al. this approach seems to have a broader acceptance from the research community. Based on the broader acceptance within the research community and the promising validations by Ge et al. and Tippmann et al. the Arora approach will be used also in this project. In the following subsection the mathematical formulation of lithium plating will be presented.

Mathematical Formulation of Lithium Plating

The two processes needed to account for when modeling lithium plating are the electron charge transfer happening in the reaction $\text{Li}^+ + \text{e}^- \rightarrow \text{Li(s)}$, which is assumed in this model to first form near the electrode-separator interface during overcharge and the change in resistance due to the film formed by insoluble products. These two processes are described mathematically below.

The Lithium Plating Reaction

Recalling the charge transfer reaction from equation 3.20, the reaction rate of lithium deposition could be related to the overpotential by the Butler-Volmer equation (equation 3.24). It is assumed that the process of lithium deposition is semi-reversible. This means that both the forward and backward reaction is considered when the overpotential for the reaction is negative. However, no lithium plating reaction is allowed to occur when the overpotential is positive.

$$I_{Li} = \min \left(0, i_{Li,0} \left[\exp \left(\frac{\alpha_a F}{RT} \eta_{Li} \right) - \exp \left(-\frac{\alpha_c F}{RT} \eta_{Li} \right) \right] \right) \quad (3.24)$$

Here the subscript Li refers to lithium plating. The surface overpotential η_{Li} and the exchange current density $i_{Li,0}$ is defined in equation 3.25 and 3.26 respectively. The minimum function is used to consider the semi-reversibility of the lithium plating reaction.

$$\eta_{Li} = \Phi_1 - \Phi_2 - U_{Li} - I_{Li}R_{film} \quad (3.25)$$

$$i_{0,Li} = Fk_{Li,a}^{\alpha_{Li,c}}k_{Li,c}^{\alpha_{Li,a}}c_2^{\alpha_{Li,a}} \quad (3.26)$$

Here the overpotential U_{Li} with respect to Li/Li^+ will be zero and R_{film} is the resistance caused by the SEI layer and the film formed as a result of lithium plating (equation 3.27).

Change in Film Resistance due to Lithium Plating

Once formed the deposited metallic lithium on the negative electrode will react with the surrounding electrolyte and create insoluble products. Even though many products will form, only Li_2CO_3 is considered as an approximation [17]. This approximation has not been further investigated in this project. In resemblance with the SEI the insoluble products create a thin film around the electrode and protect the metallic lithium from further reaction with the solvent. The film resistance R_{film} is calculated as the sum of the resistance from the SEI layer R_{SEI} and the resistance from the products formed by lithium plating $R_{products}$ (equation 3.27). A schematic figure illustrating the different resistances can be found below (figure 3.2).

In this figure lithium (green) has deposited on the particle surface and metallic lithium has reacted with the surrounding liquid to create a film (light grey). These two represent the resistance $R_{products}$. All are surrounded by the SEI (dark gray) which represent the resistance R_{SEI} .

$$R_{film} = R_{SEI} + R_{products} \quad (3.27)$$

Since SEI growth is not accounted for in this project the thickness of the SEI is taken to be constant. R_{SEI} is calculated as a function of the SEI thickness δ_{SEI} , the ionic conductivity κ_{SEI} and the electrode surface area A_i for electrode i (equation 3.28).

$$R_{SEI} = \frac{\delta_{SEI}}{\kappa_{SEI}A_i} \quad (3.28)$$

To calculate the change in film resistance due to lithium plating $R_{products}$, an expression for the film thickness is needed. The material balance of the metallic lithium

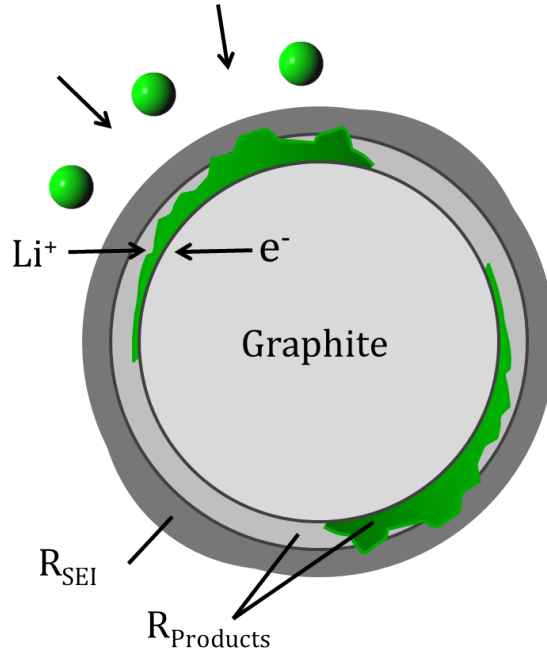


Figure 3.2: A schematic figure illustrating the film surrounding the active material particle.

is expressed by the general material balance equation (equation 3.1). For solids a good approximation will be to set the net molar flux $\nabla N = 0$. This will reduce the material balance for metallic lithium to only production (equation 3.29).

$$\frac{\partial c_{Li}}{\partial t} = -a \frac{I_{Li}}{F} \quad (3.29)$$

Equation 3.29 could be rewritten in terms of the thickness of the produced film $\delta_{products}$ (equation 3.30).

$$\frac{\partial \delta_{products}}{\partial t} = -\frac{M I_{Li}}{\rho F} \quad (3.30)$$

Here M is the average molar mass and ρ is the density of the species in the film.

The resistance of the formed film ($R_{products}$) can be calculated by equation 3.31.

$$R_{products} = \varepsilon_{Li} \frac{\delta_{products}}{\kappa_{Li} A_i} + \varepsilon_{Li_2CO_3} \frac{\delta_{products}}{\kappa_{Li_2CO_3} A_i} \quad (3.31)$$

4

Method

The equations presented in Modeling Lithium-ion Batteries needs to be solved simultaneously. This was done by Newman et al. who developed a subroutine called BAND (J) in FORTRAN [23]. However, in this project the derivatives in the governing equations are discretized and the governing equations are rewritten as resistances and potentials in an equivalent electric circuit in Simulink. This approach makes it easy to get an overview of the model and to expand the model to include more processes (such as lithium plating) by time.

This chapter will include an explanation of the spatial discretization of the model and a schematic drawing of the electric circuit network. It will also include the transformation of the governing equations to resistances and potentials and the temperature dependence and the calculation procedure used in the model.

4.1 Model Dimensions

In the model the electrodes are split into three domains each and the separator is treated as one domain. Each domain is split into six elements, which means that the whole electrochemical cell is discretized in 42 elements, (figure 4.1). The model is pseudo two dimensional, with the second dimension taken as the radii of the particle spheres. The spheres are discretized by split in six shells of equal length ($R_s/6$) (figure 4.2).

The different naming of elements and domains is used since different calculations are done at different level of discretization. At the element-level the concentrations in the cell are calculated while the remaining calculations are done at the domain-level using the average concentration.

The choice of using the right discretization is a balance between simulation time and accuracy. However, the dimensions in the model have been inherited from the development of the original model and have not been investigated within the scope of this project.

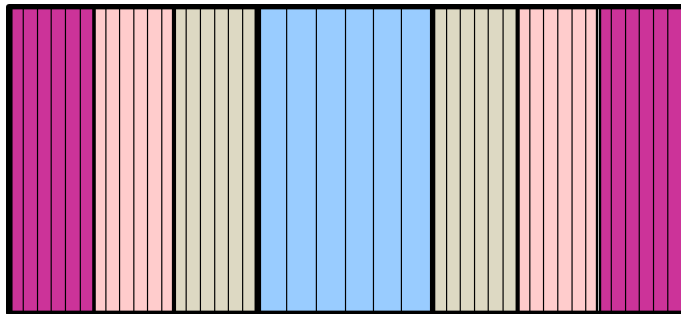


Figure 4.1: The discretization of the cell. The blue domain represents the separator with the positive electrode to its left and the negative electrode to the right.

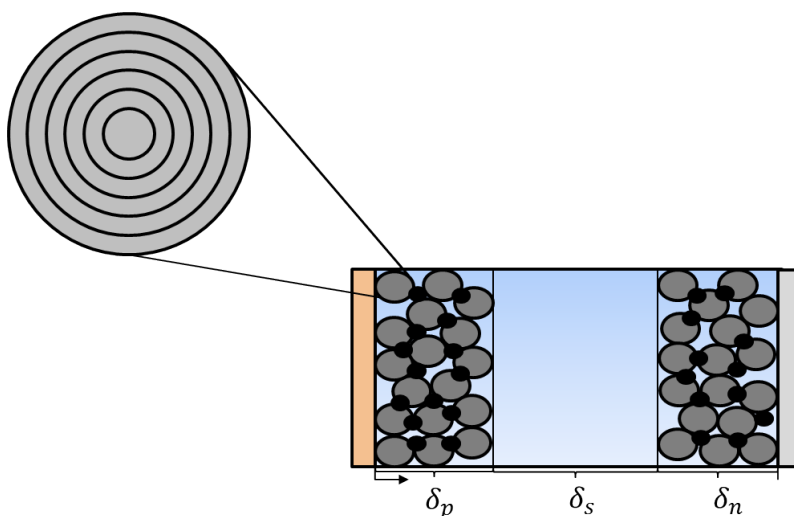


Figure 4.2: The discretization of the active material spheres.

4.2 The Electric Circuit Network

A schematic drawing of the electric circuit network can be seen in figure 4.3. The left side of the figure (subscript p) corresponds to the processes in each domain (subscript 1, 2 and 3) in the positive electrode. Each box includes two parallel branches, which can be seen in the schematic drawing as the links between the boxes. The upper branch includes the resistance accounting for the electronic transport in the active material. The lower branch include the resistance and potential that arise due to the ionic current in the electrolyte. The two branches are coupled via resistances and voltages related to the charge transfer reaction and the transportation of Li-ions through the film surrounding the active material particles.

In the same sense the right side (subscript n) corresponds to the processes in each domain (subscript 3, 2, and 1) in the negative electrode. In this electrode the

electronic and ionic branch are coupled by both the charge transfer reaction and the lithium plating reaction as parallel processes.

The two electrodes are connected by the separator (notation *sep*). Since no electric current flow through the separator, this box only consist of one branch accounting for the resistance and potential of the ionic current in the electrolyte.

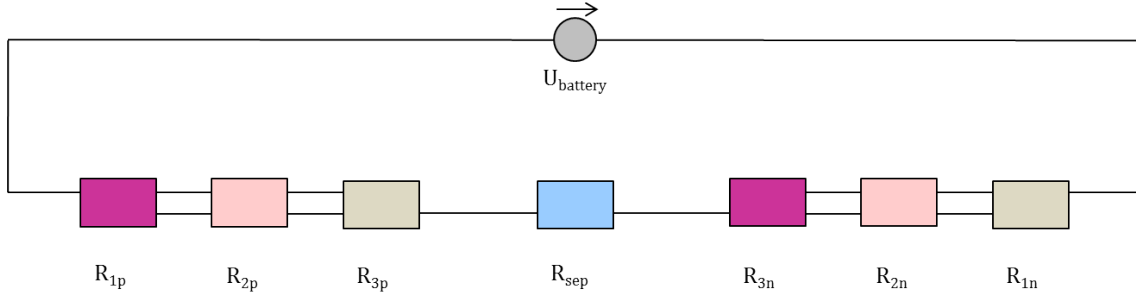


Figure 4.3: A schematic drawing of the electric circuit network.

Below an explanation of all resistances and voltages in the electric circuit network (figure 4.3) as well as how they are related to the governing equations in Modeling Lithium-ion Batteries is given.

$U_{battery}$ is the OCP in the electrochemical cell. The resistances in the upper branch correspond to the resistance that arise due to the transportation of electrons inside the positive and negative electrode and are denoted $R1$. These resistances correspond to the first term in equation 3.23 and can be derived by some rearrangements (equation 4.1). Note that the current density i_1 is multiplied by the cross-section area A to get the current.

$$\begin{aligned} \nabla\eta &= -\frac{i_1}{\sigma_{eff}} \\ \frac{\eta_{x+1} - \eta_x}{\Delta x} &= -\frac{i_1 A}{\sigma_{eff} A} \\ R1 &= \frac{\eta_{x+1} - \eta_x}{i_1 A} = -\frac{\Delta x}{\varepsilon_1^{brug} \sigma A} \end{aligned} \quad (4.1)$$

The resistances in the lower branch correspond to the ionic conductivity in the electrolyte and are denoted $R2$ and R_{sep} . These resistances are derived from the second term in equation 3.23 or the first term in equation 3.11 by transforming this term from a potential to a resistance (equation 4.2).

$$\begin{aligned}
\nabla\eta &= \frac{i_2}{\kappa_{eff}} \\
\frac{\eta_{x+1} - \eta_x}{\Delta x} &= -\frac{i_2 A}{\kappa_{eff} A} \\
R2 &= \frac{\eta_{x+1} - \eta_x}{i_2 A} = -\frac{\Delta x}{\varepsilon_2^{brug} \kappa A}
\end{aligned} \tag{4.2}$$

The lower branch also includes voltages. These voltages are denoted U_{conc} and are polarization potentials caused by local concentration differences and corresponds to the third and fourth term of equation 3.23. This equation has been discretized and in the model the voltages are described by equation 4.3.

$$U_{conc} = \frac{2RT}{F} \left(1 - t_+^0(c)\right) \ln \frac{c_{x+1}}{c_x} \tag{4.3}$$

The electric current (the upper branch) and the ionic current (the lower branch) are coupled via the charge transfer reaction and the lithium plating reaction. The resistance associated with the electron charge transfer in the intercalation reaction $\text{Li} \rightleftharpoons \text{Li}^+ + \text{e}^-$ is denoted RCT , while the resistances associated with the competing lithium plating reaction $\text{Li} \rightarrow \text{Li}^+ + \text{e}^-$ is denoted RLi . To find the resistances RCT and RLi the Butler Volmer equation is used (equation 3.20 and 3.24). The potentials η_s and η_{Li} are replaced with the charge transfer currents ICT and ILi multiplied with RCT and RLi respectively by the use of Ohm's law. To calculate the resistances the Newton iteration method is used to find the root of equation 4.4 and 4.5. Equation 4.6 is used as convergence criteria for the iteration.

$$f(RCT) = ICT - i_0 \left[\exp\left(\frac{\alpha_a F}{RT} ICT \cdot RCT\right) - \exp\left(-\frac{\alpha_c F}{RT} ICT \cdot RCT\right) \right] \tag{4.4}$$

$$f(RLi) = ILi - \min\left(0, i_{Li,0} \left[\exp\left(\frac{\alpha_a F}{RT} ILi \cdot RLi\right) - \exp\left(-\frac{\alpha_c F}{RT} ILi \cdot RLi\right) \right]\right) \tag{4.5}$$

$$\left| \frac{f(R)f''(R)}{f'(R)^2} \right| < 1 \tag{4.6}$$

When crossing between the upper and lower branch, Li-ions also need to flow through the film surrounding the active material particles. This resistance is denoted, R_{film} ,

and contains the SEI layer and the layer formed by lithium plating. The expression for these resistances can be found in equation 3.27.

The OCP for each electrode, denoted U , are accounted for by adding this potential in series with the charge transfer resistance and the film resistance. These potentials will vary with concentration and different active materials and are usually determined by fitting a function to experimental data, see Validation of Model. For the lithium plating reaction the potential of lithium metal, denoted ULi is used instead of the OCP for the negative electrode. These voltages are simply put to zero.

By using Kirchhoff's laws and the branch current method a system of equations can be found to describe the electric circuit network (equation 4.8).

4.3 Temperature Dependence

To make accurate simulations at low temperatures an Arrhenius dependence is introduced on the reaction rate constants k_n , k_p and k_{Li} , the ionic conductivity κ_2 and the diffusion coefficients D_2 , $D_{a,n}$ and $D_{a,p}$ (equation 4.7). The OCP-curves for the two electrodes also depend on temperature. This temperature dependence is accounted for in the validation with Tippmann et al. by equation 5.6 and not by the Arrhenius equation 4.7.

$$X(T) = X(T_{ref}) \exp\left(\frac{E_{act,X}}{R} \left(\frac{1}{T_{ref}} - \frac{1}{T}\right)\right) \quad (4.7)$$

Here X is the temperature dependent parameter and $E_{act,X}$ is the activation energy of X . T_{ref} is the reference temperature at which the parameter value is given.

$$\begin{aligned}
\left\{ \begin{aligned}
U_{battery} &= (R1_{1n} + R1_{2n} + R1_{3n} + RLi_{3n} + Rfilm_{3n} + R2_{3n} + Rsep + R2_{3p} + Rfilm_{3p} + RCT_{3p} + R1_{3p} + R1_{2p} + R1_{1p})I_{battery} \\
&\quad + (-R1_{2p})I_1 + (-RCT_{3p} - Rfilm_{3p} - R1_{3p})I_2 + (-RLi_{3n} - Rfilm_{3n})I_3 + (-R1_{3n})I_4 + (-R1_{2n})I_6 \\
-U_{1p} + U_{2p} + Ucon_{c_{21p}} &= -R1_{2p}I_{battery} + (RCT_{1p} + Rfilm_{1p} + R2_{1p} + Rfilm_{2p} + RCT_{2p} + R1_{2p})I_1 + (-RCT_{2p} - Rfilm_{2p})I_2 \\
-U_{2p} + U_{3p} + Ucon_{c_{32p}} &= (-RCT_{3p} - R1_{3p} - Rfilm_{3p})I_{battery} + (-RCT_{2p} - Rfilm_{2p})I_1 + (RCT_{2p} + Rfilm_{2p} + R2_{2p} + \\
&\quad Rfilm_{3p} + RCT_{3p} + R1_{3p})I_2 \\
U_{3n} - ULi_{3n} &= (-RLi_{3n} - Rfilm_{3n})I_{battery} + (RCT_{3n} + 2Rfilm_{3n} + RLi_{3n})I_3 + (-RCT_{3n} - Rfilm_{3n})I_4 \\
-U_{3n} + ULi_{2n} + Ucon_{c_{23n}} &= -R1_{3n}I_{battery} + (-RCT_{3n} - Rfilm_{3n})I_3 + (R1_{3n} + RLi_{2n} + Rfilm_{2n} + R2_{2n} + Rfilm_{3n} \\
&\quad + RCT_{3n})I_4 + (-RLi_{2n} - Rfilm_{2n})I_5 \\
U_{2n} - ULi_{2n} &= (-Rfilm_{2n} - RLi_{2n})I_4 + (RCT_{2n} + 2Rfilm_{2n} + RLi_{2n})I_5 + (-RCT_{2n} - Rfilm_{2n})I_6 \\
-U_{2n} + ULi_{1n} + Ucon_{c_{12n}} &= (-R1_{2n})I_{battery} + (-RCT_{2n} - Rfilm_{2n})I_5 + (R1_{2n} + RLi_{1n} + Rfilm_{1n} + R2_{1n} \\
&\quad + Rfilm_{2n} + RCT_{2n})I_6 + (-RLi_{1n} - Rfilm_{1n})I_7 \\
U_{1n} - ULi_{1n} &= (-RLi_{1n} - Rfilm_{1n})I_6 + (RCT_{1n} + 2Rfilm_{1n} + RLi_{1n})I_7
\end{aligned} \right. \quad (4.8)
\end{aligned}$$

The system of equations above is used to describe the electric circuit network and is derived using the branch current method. The first equation in the system corresponds to a loop through the whole battery and the remaining equations correspond to loops so that each reaction path is included at least once. The relationships between I_1, I_2, \dots, I_7 and the currents in the different parts of the network are listed below:

$$\begin{aligned}
I1_{1p} &= I_{battery} & I1_{2p} &= I_{battery} - I_1 & I1_{3p} &= I_{battery} - I_2 & I1_{3n} &= I_{battery} - I_4 & I1_{2n} &= I_{battery} - I_6 & I1_{1n} &= I_{battery} \\
ICT_{1p} &= I_1 & ICT_{2p} &= I_2 - I_1 & ICT_{3p} &= I_{battery} - I_2 & ICT_{3n} &= I_3 - I_4 & ICT_{2n} &= I_5 - I_6 & ICT_{1n} &= I_7 \\
I2_{1p} &= I_1 & I2_{2p} &= I_2 & I2_{3p} &= I_{battery} & I2_{3n} &= I_{battery} & I2_{2n} &= I_4 & I2_{1n} &= I_6 \\
&&&&&&&&&&&&& ILLi_{3n} &= I_{battery} - I_3 & ILLi_{2n} &= I_4 - I_5 & ILLi_{1n} &= I_6 - I_7
\end{aligned}$$

4.4 Calculation procedure

The calculation procedure in the model is shown in figure 4.4. The model input (marked with a blue arrow in the figure) is the charging current or the wanted discharge current. The iteration can be followed by following the arrows from the previous step. In the first iteration the input is used to solve the electric circuit network as a set of linear equations (equation 4.8). The results from these calculations are the currents in all parts of the battery cell, denoted I_{vec} . In the next step these currents are used together with the material balance for the active material particles (equation 3.17) and the material balance for the electrolyte (equation 3.12 and 3.9) to calculate new concentrations in the battery cell. These concentrations are later used to calculate new resistances and potentials in the electric circuit network, which are used for the next iteration. A common charging strategy is constant current charging (CC) to a cut-off voltage and after that constant voltage charging (CV). The model allows for this by also including a cut-off voltage as input. If the cut-off voltage is reached the electric circuit network is solved with the cut-off voltage as input instead of the wanted current.

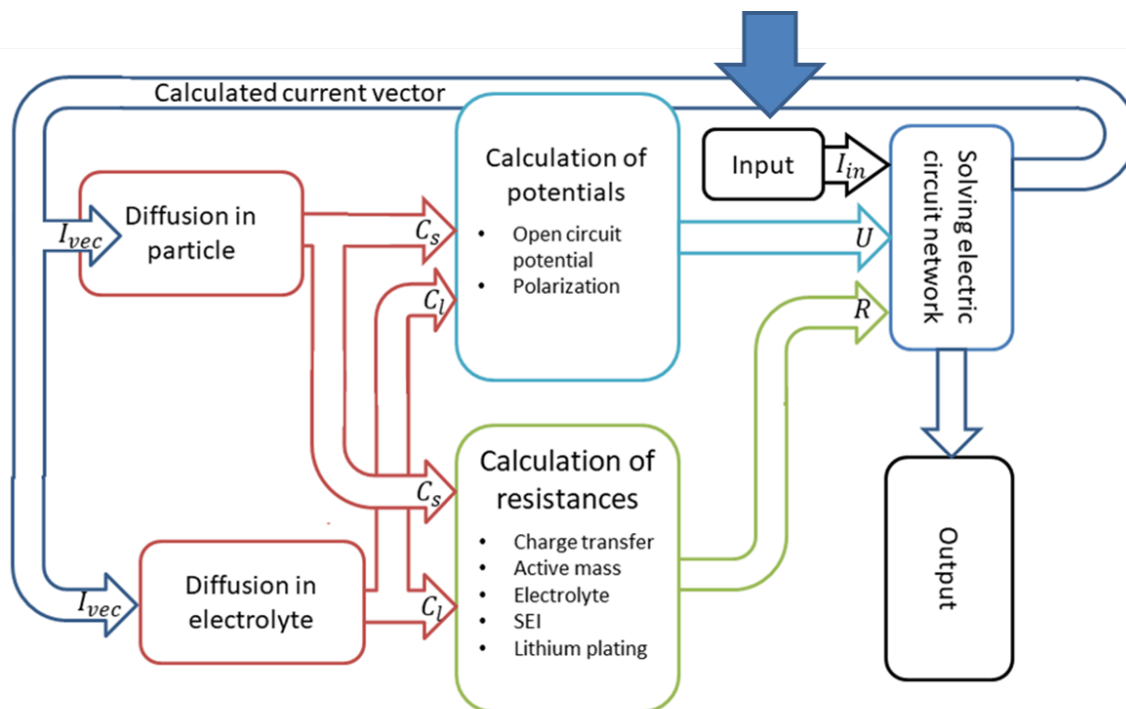


Figure 4.4: A schematic picture over the calculation procedure in the model.

5

Validation of Model

The model has been validated by comparison with other models for lithium plating (Arora et al. and Tippmann et al.) and with a few experimental data points (Tippmann et al.). This chapter presents all parameters used as well as the results of the comparisons. A sensitivity analysis is also included in order to get an understanding of which parameters that have the greatest impact on the results.

5.1 Comparison with Arora et al.

In the article from Arora et al. lithium plating is modeled for a Li-ion cell consisting of graphite and LMO as negative and positive electrode and an electrolyte of 1M LiPF₆ in a 2:1 wt. of ethylene carbonate and dimethyl carbonate [17]. The OCPs used for the two electrodes are presented in equation 5.1 and equation 5.2 [17, 24]. The material parameters used are listed in table 5.1. In this table the parameters given by Gozdz et al. (reference [24]) are also used by Arora et al.

$$U_n = 0.7222 + 0.13868\psi_n + 0.028952\psi_n^{0.5} - 0.017189\psi_n^{-0.5} + 0.0019144\psi_n^{-1.5} + 0.28082 \exp(15(0.06 - \psi_n)) - 0.79844 \exp(0.44649(\psi_n - 0.92)) \quad (5.1)$$

Here $\psi_i = c_i/c_{\tau,i}$ is the dimensionless concentration in the electrode. In these simulations $\psi_n^{0\%} = 0.1$ when fully discharged and $\psi_n^{100\%} = 0.9$ when fully charged[25].

$$U_p = 4.19829 + 0.0565661 \tanh(-14.5546\psi_p + 8.60942) - 0.0275479 \left[\frac{1}{(0.998432 - \psi_p)^{0.492465}} - 1.90111 \right] - 0.157123 \exp(-0.04738\psi^8) + 0.810239 \exp(-40(\psi_p - 0.133875)) \quad (5.2)$$

In these simulations $\psi_p^{0\%} = 0.95$ when fully discharged and $\psi_p^{100\%} = 0.175$ when fully charged[25].

Table 5.1: Parameters used in the comparison with Arora et al.

Parameter	Anode	Separator	Cathode
Thickness δ [μm]	80/85/99 ^{a*}	76.2[25]	179.3*
Thickness δ_{SEI} [μm]	0**	-	0**
Particle radius R_s [μm]	12.5*	-	8.5*
Porosity ϵ_a	0.59[25]	0[25]	0.534[25]
Max. concentration c_τ [mol/dm^3]	30.54*	-	22.86*
Electric conductivity σ [S/m]	100*	-	3.8*
Transfer coefficient α_a/α_c	0.5/0.5*	-	0.5/0.5*
Transfer coefficient $\alpha_{Li,a}/\alpha_{Li,c}$	0.7/0.3*	-	-
Transference number t_+^0	0.363[24]	0.363[24]	0.363[24]
Start concentration c_2 [mol/m^3]	1000*	1000*	1000*
Bruggeman factor $brug_2$	1.5[25]	1.0[25]	1.5[25]
Bruggeman factor $brug_a$	1.5**	-	1.5**
Ionic conductivity $\kappa_{Li}/\kappa_{Li_2CO_3}$ [S/m]	$10^6/1.2 \cdot 10^{-6}$ [21]	-	-
Volume fraction z_{Li}	1**	-	-
Diffusion coefficient D_a [m^2/s]	$2 \cdot 10^{-14}$ *	-	$1 \cdot 10^{-13}$ *
Diffusion coefficient D_2 [m^2/s]	$7.5 \cdot 10^{-11}$ *	$7.5 \cdot 10^{-11}$ *	$7.5 \cdot 10^{-11}$ *
Exchange current density i_0 [A/m^2]	2.1*	-	1.3*
Exchange current density $i_{0,Li}$ [A/m^2]	10*	-	-
Ionic conductivity κ_2 [S/m]	Eq. 5.3[24]	Eq. 5.3[24]	Eq. 5.3[24]

* Parameter is given by Arora et al. [17]

** Estimated

^a used for 0%/5%/19% excess capacity.

The concentration dependence of the ionic conductivity κ_2 is accounted for by the equation 5.3 [24]. The relation between the exchange current density for the intercalation reaction i_0 and the lithium plating reaction $i_{0,Li}$ is expressed in equation 3.22 and 3.26.

$$\begin{aligned} \kappa_2 = & 1.0793 \cdot 10^{-4} + 6.7461 \cdot 10^{-3}c_2 - 5.2245 \cdot 10^{-3}c_2^2 \\ & + 1.3605 \cdot 10^{-3}c_2^3 - 1.1724 \cdot 10^{-4}c_2^4 \end{aligned} \quad (5.3)$$

A comparison between the predicted results of the developed model and the paper can be seen in the figure 5.1. In this figure the thickness of deposited lithium is modeled at different charging rates and different excess capacities in the negative electrode. The blue curve represents a charging current of $3.906 \text{ mA}/\text{cm}^2$ and excess capacity of 5%, the red $2.906 \text{ mA}/\text{cm}^2$ and 0% excess and the green a charging current of $2.906 \text{ mA}/\text{cm}^2$ and 5% excess. The charging current $2.906 \text{ mA}/\text{cm}^2$ corresponds to $\sim 1\text{C}$. The differences in onset of lithium plating between the two models are about five minutes.

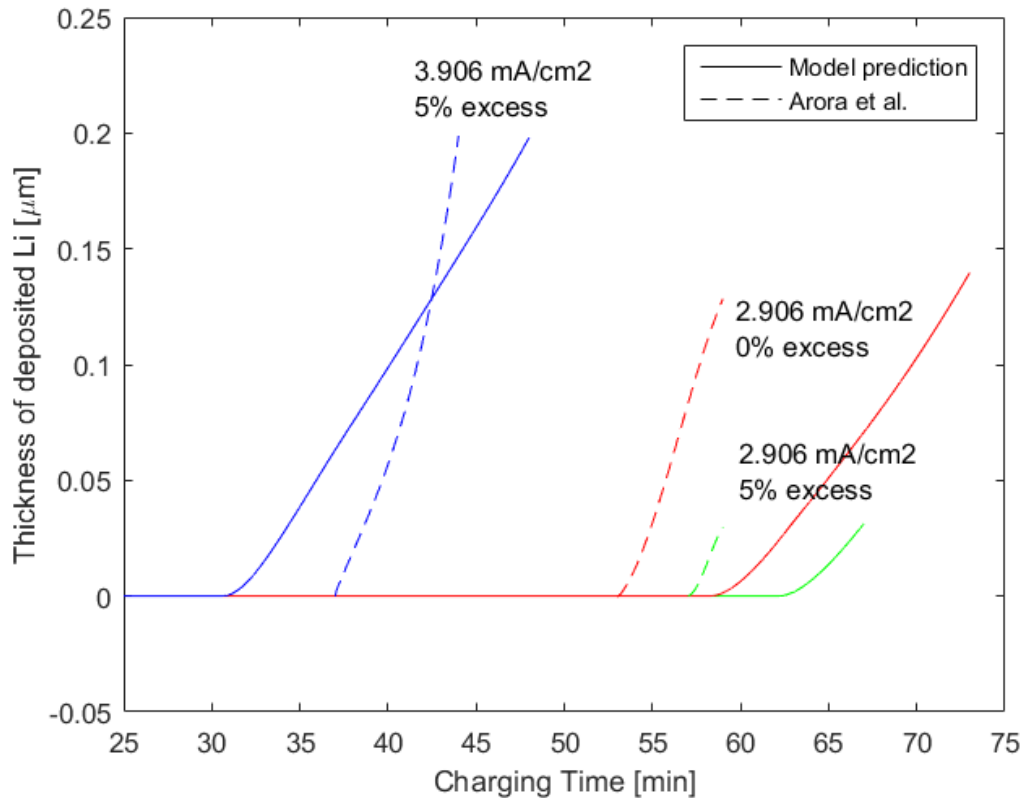
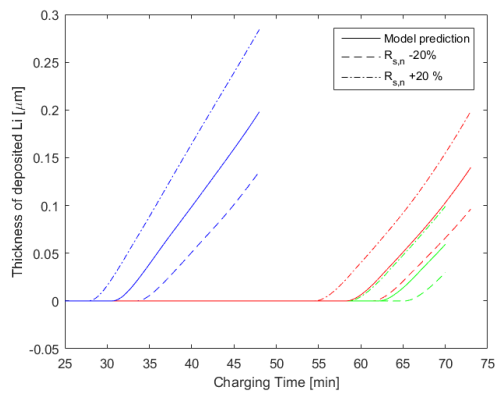


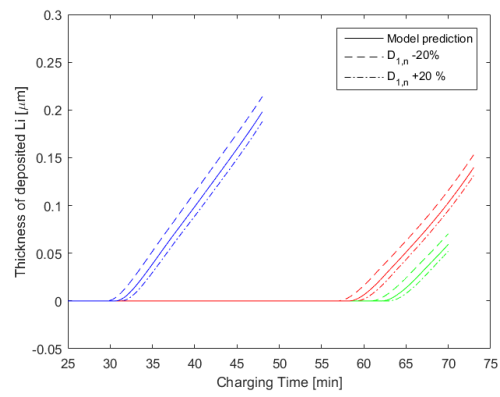
Figure 5.1: Thickness of the deposited lithium-film as a function of time for different charging currents and excess capacities in the negative electrode.

A sensitivity analysis has been conducted for some chosen material parameters in the comparison with Arora et al. by varying the parameters by $\pm 20\%$. The material parameters tested are the particle radius R_s , the diffusion coefficients $D_{1,n}$, $D_{1,p}$ and D_2 , the reaction rate coefficients k_n , k_p and k_{Li} , the ionic conductivity κ_2 , the activation energy for k_n and κ_n , the separator thickness, as well as the volume fraction ϵ_a . The sensitivity analysis for the separator thickness and the volume fraction ϵ_a are included here, but not in the sensitivity analysis of Tippmann et al. since these parameters are missing in the article by Arora et al. The OCPs have also been tested by adding $\pm 0.01V$. The sensitivity analysis was done for the same cases as in figure 5.1. The parameters which had a noticeable effect on the result are presented below (figure 5.2 and 5.3). In the sensitivity analysis for the diffusion coefficient D_2 (figure 5.2c) the blue curve for $D_2 - 20\%$ and charging current 3.906 mA/cm^2 seems to be missing. The reason why that case is not shown in the graph is that the low diffusion coefficient and the high charging current cause the concentration of Li-ions in the electrolyte in the negative electrode to fall down to zero, which cause the model to crash. In fact lithium plating occur after ~ 21.5 minutes in this case, but the model crashes shortly after this.

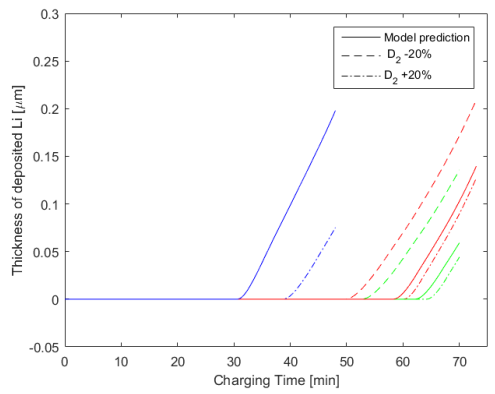
5. Validation of Model



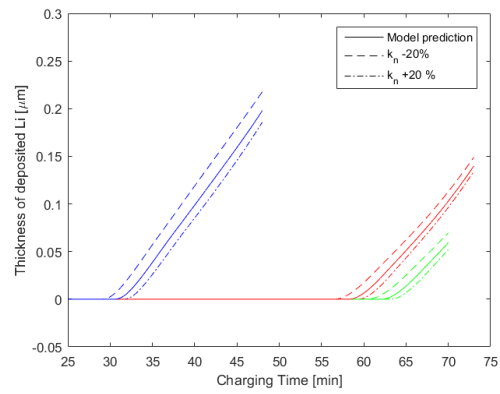
(a)



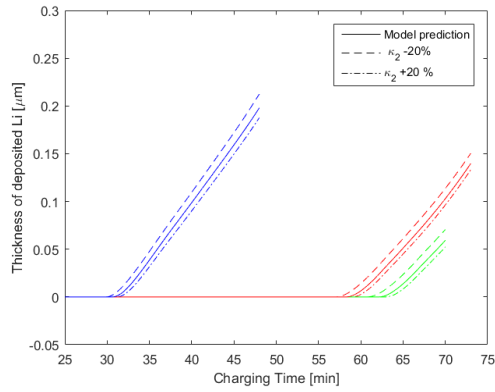
(b)



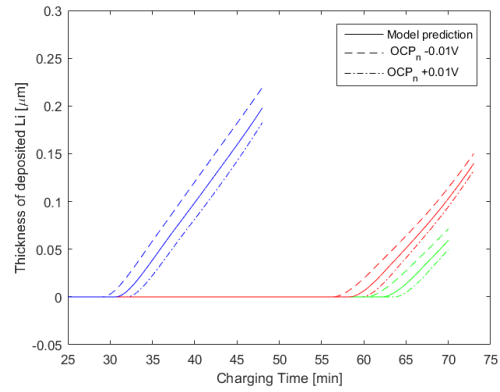
(c)



(d)



(e)



(f)

Figure 5.2: A sensitivity analysis of the material parameters used in the comparison with Arora et al.

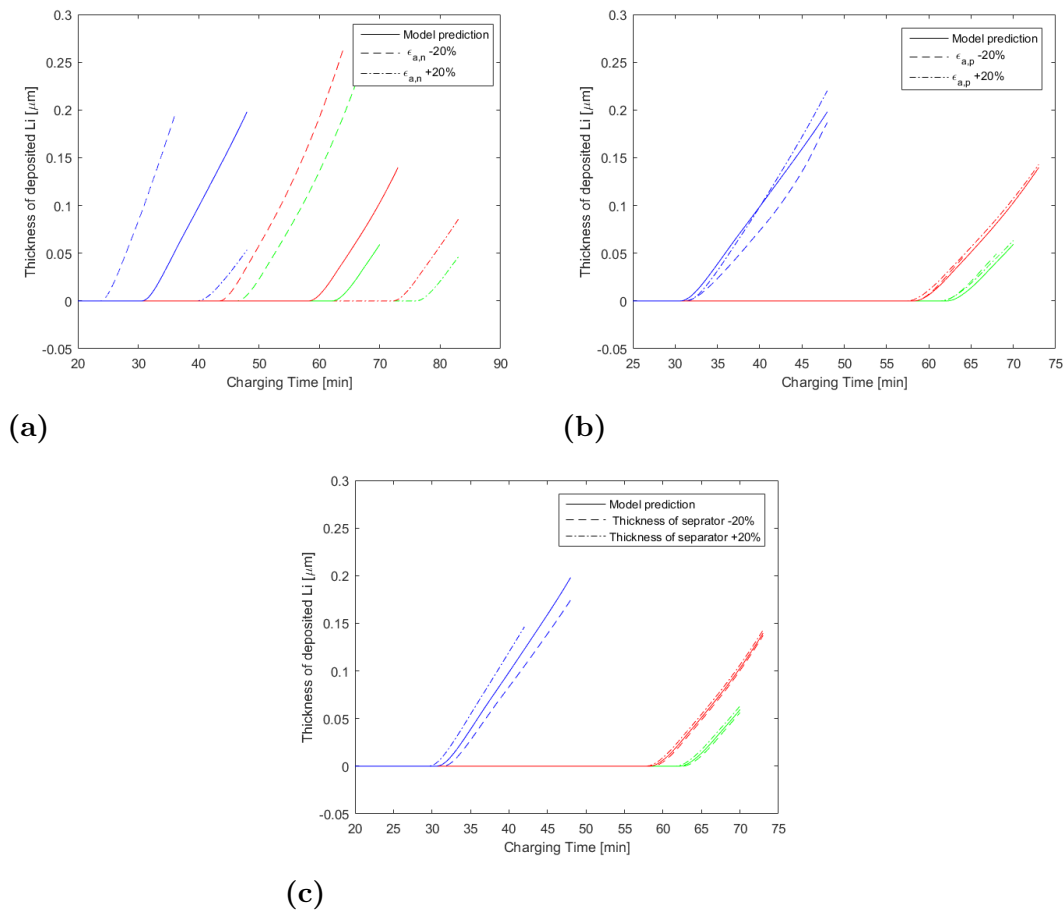


Figure 5.3: A sensitivity analysis of the material parameters used in the comparison with Arora et al.

5.2 Comparison with Tippmann et al.

In the article from Tippmann et al. [22] a Li-ion cell consisting of graphite and NMC as negative and positive electrode is modelled. The OCPs for the two electrodes can be seen in equation 5.4 and 5.5 [22]. The temperature dependence of the two OCPs are accounted for by adding the temperature dependence in equation 5.6 to the OCP of the positive electrode. The material parameters used in the comparison are listed in table 5.2 and 5.3. The parameters listed in table 5.3 are temperature dependent and are used with equation 4.7 in the model. The concentration dependence of the ionic conductivity κ_2 and the diffusion coefficient D_2 is accounted for by the equation 5.7 and 5.8.

$$U_n = \frac{-2137\psi_n^3 + 1841\psi_n^2 + 107.44\psi_n + 12.85}{\psi_n^4 - 15113\psi_n^3 + 16128\psi_n^2 + 436.68\psi_n + 10.71} \quad \text{where} \quad \psi_n = \frac{c_n}{c_{\tau,n}} \quad (5.4)$$

The dimensionless concentration of lithium in the graphite electrode is $\psi_n^{0\%} = 0.07$ when fully discharged and $\psi_n^{100\%} = 0.61$ when fully charged.

$$U_p = \frac{-3249\psi_p^3 + 10789\psi_p^2 - 9090\psi_p + 2929}{\psi_p^4 - 532\psi_p^3 + 2088\psi_p^2 - 1767\psi_p + 587} \quad \text{where} \quad \psi_p = \frac{c_p}{c_{\tau,p}} \quad (5.5)$$

The dimensionless concentration of lithium in the NMC electrode is $\psi_n^{0\%} = 0.98$ when fully discharged and $\psi_n^{100\%} = 0.48$ when fully charged.

$$\frac{\partial U_p}{\partial T} = 0.062\psi_p^4 - 0.1913\psi_p^3 + 0.2133\psi_p^2 - 0.1022\psi_p + 0.0179 \quad (5.6)$$

$$\kappa_2 = 1.0416c_2^{-0.1882} \exp\left(-0.9615 \log(c_2)^2\right) \quad (5.7)$$

$$D_2 = 3.4815 \cdot 10^{-10} \exp\left(\frac{-0.55c_2}{1000}\right) \quad (5.8)$$

Table 5.2: Parameters used in the comparison with Tippmann et al.

Parameter	Anode	Separator	Cathode
Thickness δ [μm]	65*	28*	54*
Thickness δ_{SEI} [μm]	0**	-	0**
Particle radius R_s [μm]	10*	-	10*
Porosity ϵ_a	0.62*	0.52*	0.49*
Max. concentration c_τ [mol/dm^3]	31.363*	-	51.385*
Electric conductivity σ [S/m]	0.4*	-	100*
Transfer coefficient α_a/α_c	0.5/0.5*	-	0.5/0.5*
Transfer coefficient $\alpha_{Li,a}/\alpha_{Li,c}$	0.7/0.3[17]	-	-
Transference number t_+	0.363*	0.363*	0.363*
Diffusion coefficient D [m^2/s]	table 5.3*	table 5.3*	$4 \cdot 10^{-11}$ *
Start concentration c_2 [mol/m^3]	1100*	1100*	1100*
Bruggeman factor $brug_2$	1.5**	1.5**	1.5**
Bruggeman factor $brug_a$	1.5**	-	1.5**
Ionic conductivity $\kappa_{Li}/\kappa_{Li_2CO_3}$ [S/m]	$10^6/1.2 \cdot 10^{-6}$ [21]	-	-
Volume fraction z_{Li}	0.5**	-	-
* Parameter is given by Tippmann et al. [22]			
** Estimated			

Table 5.3: Temperature dependent parameters used in the comparison with Tippmann et al.

Parameter	Value at 25°C	Activation energy [KJ/mol]
$D_{a,n}$ [m^2/s]	$3.46 \cdot 10^{-14}$ *	32.73*
k_n [m/s]	$4.57 \cdot 10^{-8}$ **	76.80*
k_p [m/s]	$4.57 \cdot 10^{-8}$ **	76.80**
k_{Li} [$mol^{0.7}/m^{1.1}s$]	$1.27 \cdot 10^{-5}$ [17]	35.30[17]
κ_2 [S/m]	Equation 5.7*	17.44*
D_2 [m^2/S]	Equation 5.8*	9.80*

* Calculated from Tippmann et al.

** Fitted to Tippmann et al.

The reaction rate coefficients by Tippmann et al. were $k_n = 1178 \exp(-9237/T)$ and $k_p = 3.6 \exp(-9616/T)$. However, since k_p is very low the resistance when using this expression becomes so large that it becomes impossible to run the model without reaching the cut-off voltage at once. Also the dimensions in the given expression for the exchange current density does not add up. Therefore the reaction rate coefficients are fitted to get the same anode potential at 0°C as Tippmann et al. did (figure 5.4). Instead of the expression for the exchange current density used in Tippmann et al. another expression is used to match the dimensions (equation 5.9). The relation between the exchange current density and the reaction rate coefficients for the lithium plating reaction is expressed in equation 3.26.

$$i_0 = Fk(c_\tau - c_a)^{\alpha_p} c_a^{\alpha_n} \left(\frac{c_2}{c_2^{ref}} \right) \quad (5.9)$$

A comparison between the two models can be seen in figure 5.5 and 5.6. In the first of these figures the onset of lithium plating is plotted as a function of charging current and temperature. This means that lithium plating is predicted to happen in the region above the curves while lithium plating is predicted to not happen under the curves. In the second figure the onset of lithium plating at $-15^\circ C$ is plotted as a function of SOC and charging current. This figure also includes data points from experiments. Noteworthy is that the model by Tippmann et al. is isothermal in figure 5.5 and include thermal effects in figure 5.6. This makes it difficult to compare the two models in figure 5.6 and is most likely the reason why the model by Tippmann et al. predicts the onset of lithium plating at higher charging currents in figure 5.6 and at lower charging currents in figure 5.5.

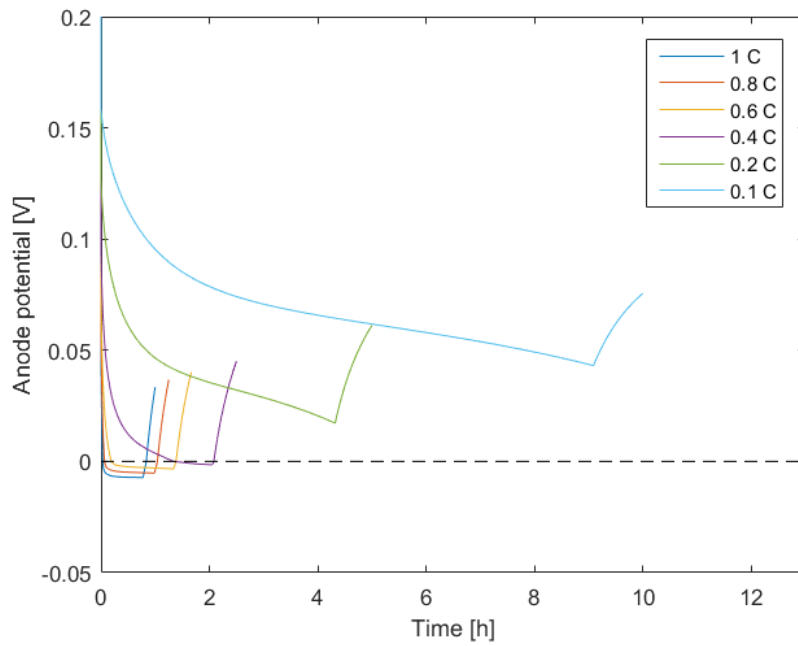


Figure 5.4: The anode potential for charging currents between 0.1C–1C at 0°C and 4.2V as cut-off voltage.

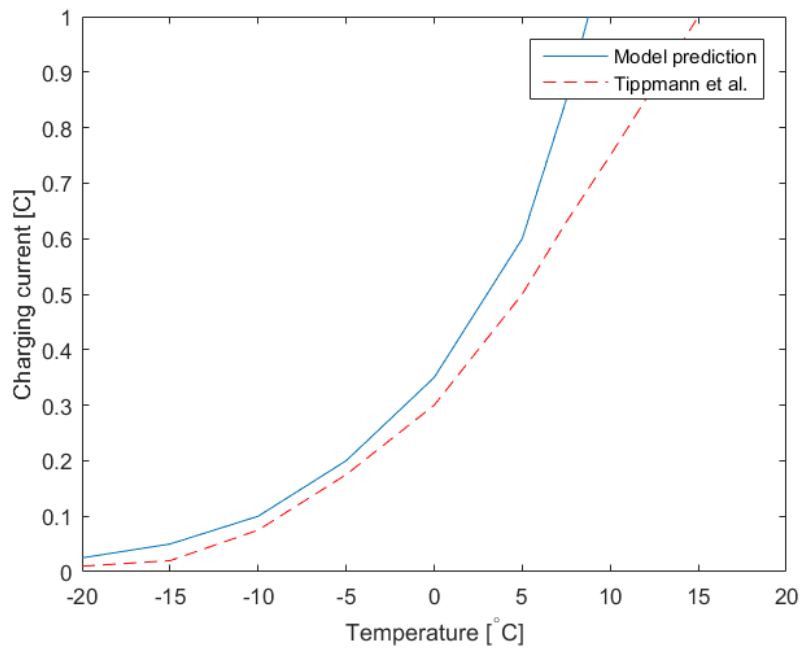


Figure 5.5: The onset of lithium plating as a function of charging current and temperature with 4.2V as cut-off voltage.

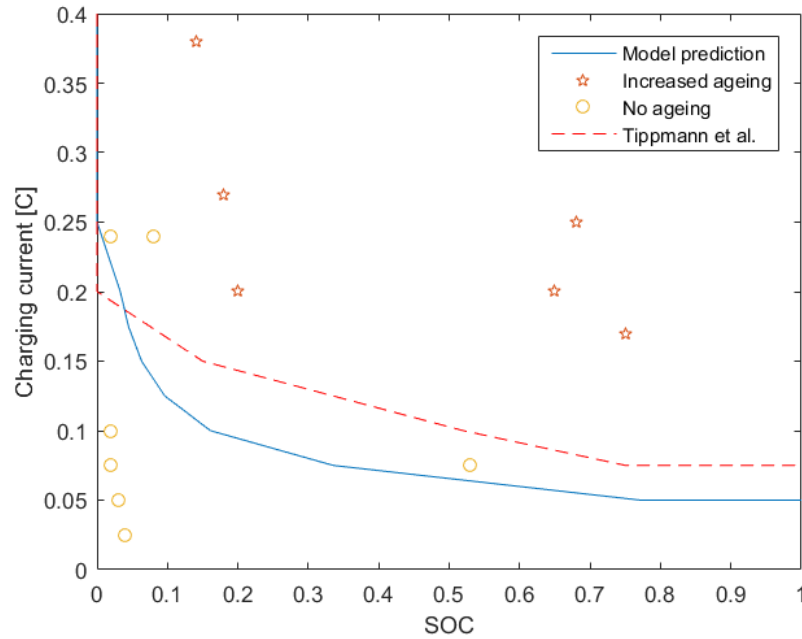


Figure 5.6: The onset of lithium plating as a function of SOC and charging current at -15°C and with 4.2V as cut-off voltage.

A sensitivity analysis has been done for the material parameters in the comparison with Tippmann et al. by varying the parameters by $\pm 20\%$ and the OCPs by ± 0.01 V under the same conditions as in figure 5.6. The material parameters tested are the particle radius R_s , the diffusion coefficients $D_{1,n}$, $D_{1,p}$ and D_2 , the reaction rate coefficients k_n , k_p and k_{Li} , the ionic conductivity κ_2 , the activation energy for k_n and κ_n and the OCPs. Parameters that had a noticeable effect on the result are presented below (figure 5.7). Noteworthy is that the three parameters R_s , k_n and the activation energy for k_n are directly linked to the charge transfer reaction.

5. Validation of Model

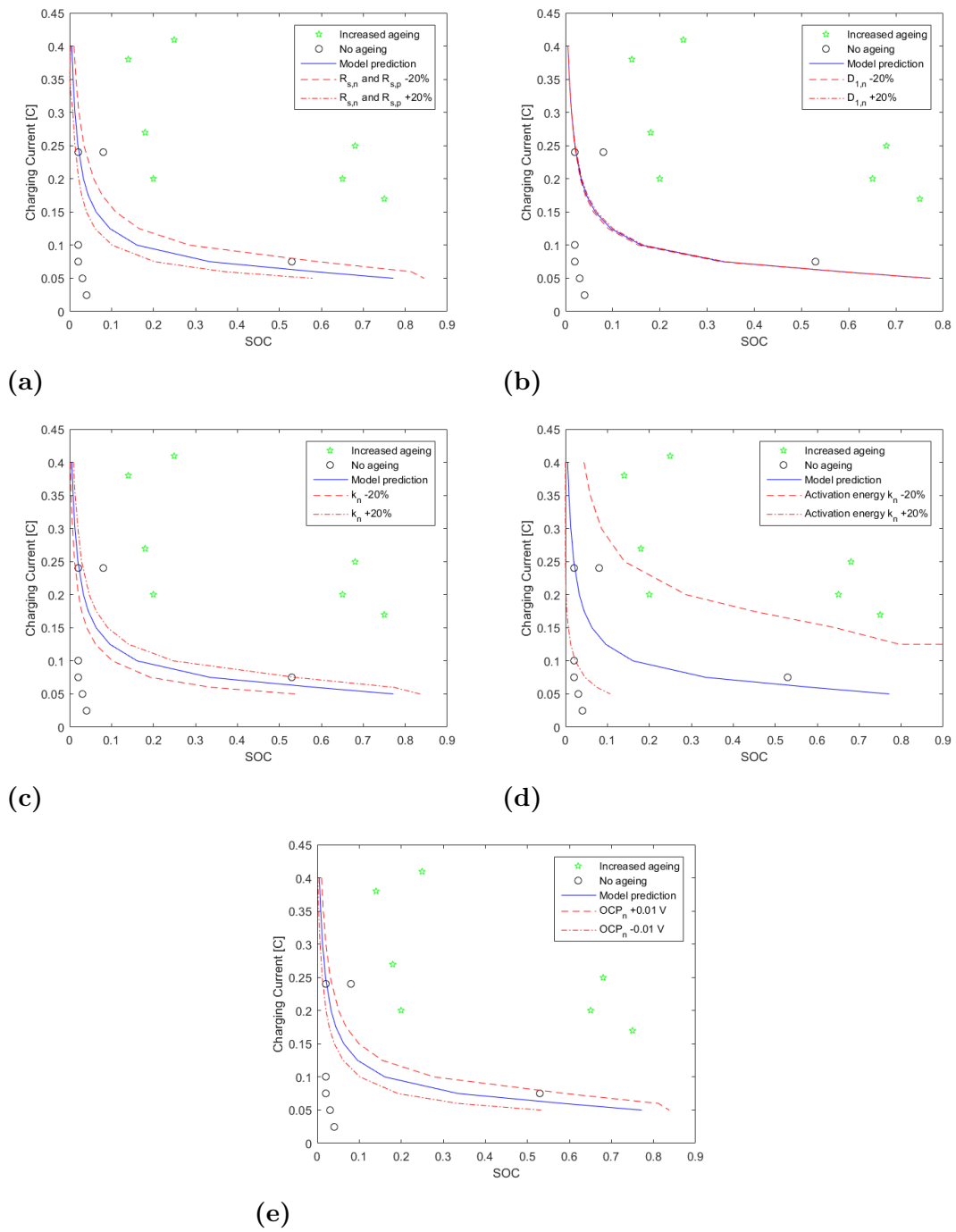


Figure 5.7: A sensitivity analysis of the material parameters used in the comparison with Tippmann et al.

6

Discussion

In this chapter the results from the validation of the model as well as the sensitivity analysis will be discussed. The comparison with the model by Arora et al. show a maximum deviation of $\sim 15\%$, or about five minutes for the onset of lithium plating (figure 5.1). It is hard to determine the reason for this deviation between the two models. However, one reason that may explain why the model presented here predict lithium plating later than Arora et al. does for the charging current 2.906 mA/cm^2 is that the predictions by Arora et al. are done at the boundary between the separator and the negative electrode. This approach makes sense since this is where the lithium plating reaction will occur first. However, this is impossible to do with the model in this project due to the inherited discretization.

In the third case (charging current 3.906 mA/cm^2 and 5% excess) the lithium plating reaction occur earlier than predicted by Arora. No explanation for this behaviour has been found. Two parameters that have been heavily discussed are the volume fraction of active material ϵ_a in the electrodes and the thickness of the separator, which are not reported in the article by Arora. Instead, these values have been found in an article by Perkins et al. who claim to summarize the parameters used by Arora [25]. The sensitivity analysis (figure 5.3) show that these parameters have a significant impact on the results. It is possible that other values for these parameters would have given a better agreement between the two models.

The comparison with the model by Tippmann et al. show a good agreement (figure 5.5 and 5.6). In this comparison, it is hard to tell which impact the fitting of the reaction rate coefficients had on the results. One concern is that the fitting of these parameters may have corrected for some error in the model. The fitting of the reaction rate parameters is crucial since the sensitivity analysis shows that k_n is one of the parameters that matters the most (figure 5.7).

In the sensitivity analysis for Tippmann et al. it is also shown that the most sensitive parameters are the ones related to the charge transfer reaction (figure 5.7). This suggests that the lithium plating occurs due to CTL under these conditions and may be why most of the other parameters do not show any impact. This is not the case in the sensitivity analysis for Arora et al. (figure 5.2 and 5.3) where many more parameters have an impact on the results. In both of the sensitivity analyzes,

it could be noted that the material parameters for the positive electrode have a very low impact on the result. This points out that efforts to determine material parameters should be focused on the negative electrode.

The model has been validated by comparing with other models and by the few experimental data points provided by Tippmann et al. However, efforts to validate the model with experimental data have also been done, but proved to be difficult for a couple of reasons:

- The first reason is that lithium plating is a phenomenon that is hard to measure experimentally and only a few articles have been found where lithium plating has been investigated experimentally.
- Secondly, physics-based models require a lot of material dependent parameters. In the articles where experimental data have been found most of the parameters needed in the model are not given. To find the parameters from other sources have proven to be difficult and reported values for some parameters also varies a lot e.g. the reaction rate coefficient may vary by a factor of 10^2 for the same cell depending on how it is measured. For cells fabricated in the lab parameters such as the porosity are impossible to find if it is not reported by the authors.

The aim of this thesis work has been to create a model for lithium plating in LIBs which can be used to predict optimal charging conditions for fast charging at low temperatures. The model has been validated by comparison with other models for charging currents over 1 C (Arora et al.) and temperatures down to -20°C (Tippmann et al.) with good agreement. Despite the lack of validation with experimental data the model seems to work and the project aim is met. However, before the model can be used to improve the charging routines in cars the material parameters and lithium plating data would need to be determined experimentally for the batteries of interest. The model would also need to be validated with the use of these parameters and data.

7

Further Work

A couple of suggestions to further improve the model are provided here, based on the current results and status. When charging at high current the internal resistance in the battery will cause heat to be generated. This heat will increase the reaction rate of the charge transfer reaction and the diffusion in the active material and thus prevent or delay lithium plating. To charge the battery as fast as possible without risking to damage the battery this effect will need to be taken into account. The first suggestion is therefore to couple a thermal model to the lithium plating model.

The discretization used in this project was inherited from a previous project and has not been tested. One suggestion to further improve the model is therefore to refine the discretization to improve accuracy. As detailed above lithium plating will happen first on the electrode-separator boundary. Since the structure of the model is built on three domains and the lithium plating current is calculated from the average concentration in each domain the model is likely to predict lithium plating later than it should. To fix this it is suggested to insert a very narrow domain on the boundary between the negative electrode and the separator.

Deposited lithium is known to form dendrites, which potentially could short-circuit the battery cell. This happens since the deposited lithium form a hot spot for lithium plating. However, this is not captured in the model. Instead the deposited lithium forms a resistance for both the lithium plating reaction and the charge transfer reaction. To fix this the resistance developed by the deposited lithium could be removed from the lithium plating branch in the electric circuit network.

Bibliography

- [1] J. Groot, *State-of-health estimation of Li-ion batteries: Ageing models*. PhD thesis, Chalmers University of Technology, 2014.
- [2] EPA, “Global greenhouse emissions data.” Accessed: 02.03.2018, <https://www.epa.gov/ghgemissions/global-greenhouse-gas-emissions-data>.
- [3] V. Cars, “Volvo cars to go all electric,” 05.07.2017. Accessed: 18.01.2018, <https://www.media.volvocars.com/global/en-gb/media/pressreleases/210058/volvo-cars-to-go-all-electric>.
- [4] X.-G. Yang, Y. Leng, G. Zhang, S. Ge, and C.-Y. Wang, “Modeling of lithium plating induced aging of lithium-ion batteries: Transition from linear to non-linear aging,” *Journal of Power Sources*, vol. 360, pp. 28–40, 2017.
- [5] A. Franco, M. L. Doublet, and W. Bessler, *Physical Multiscale Modeling and Numerical Simulation of Electrochemical Devices for Energy Conversion and Storage: From theory to engineering to practice*. Springer, 2016.
- [6] Y. Tang, Y. Zhang, W. Li, B. Ma, and X. Chen, “Rational material design for ultrafast rechargeable lithium-ion batteries,” *Chemical Society Reviews*, vol. 44, no. 17, pp. 5926–5940, 2015.
- [7] Z. Li, J. Huang, B. Y. Liaw, V. Metzler, and J. Zhang, “A review of lithium deposition in lithium-ion and lithium metal secondary batteries,” *Journal of Power Sources*, no. 254, pp. 168–182, 2014.
- [8] M. Tang, P. Albertus, and J. Newman, “Two-dimensional modeling of lithium deposition during cell charging,” *Journal of the Electrochemical Society*, vol. 156, no. 5, pp. 390–399, 2009.
- [9] Thomas Jefferson National Accelerator Facility - Office of Science Education, “It’s elemental - the element lithium.” Accessed: 11.04.2018, www.jlab.org.
- [10] L. Oliveira, M. Messagie, S. Rangaraju, J. Sanfelix, M. H. Rivas, and J. Van Mierlo, “Key issues of lithium-ion batteries—from resource depletion to

- environmental performance indicators,” *Journal of cleaner production*, vol. 108, pp. 354–362, 2015.
- [11] J. F. Peters, M. Baumann, B. Zimmermann, J. Braun, and M. Weil, “The environmental impact of li-ion batteries and the role of key parameters—a review,” *Renewable and Sustainable Energy Reviews*, vol. 67, pp. 491–506, 2017.
- [12] T. B. Reddy, *Linden’s Handbook of Batteries, Fourth Edition*. McGraw-Hill Education, 2011.
- [13] Y. Wu, *Lithium-ion batteries: Fundamentals and Applications*, vol. 4. CRC Press, 2015.
- [14] D. Andre, S.-J. Kim, P. Lamp, S. F. Lux, F. Maglia, O. Paschos, and B. Staszny, “Future generations of cathode materials: an automotive industry perspective,” *Journal of Materials Chemistry A*, vol. 3, no. 13, pp. 6709–6732, 2015.
- [15] N. Legrand, B. Knosp, P. Desprez, F. Lopicque, and S. Raël, “Physical characterization of the charging process of a li-ion battery and prediction of li plating by electrochemical modelling,” *Journal of Power Sources*, vol. 245, pp. 208–216, 2014.
- [16] M. Doyle, T. F. Fuller, and J. Newman, “Modeling of galvanostatic charge and discharge of the lithium/polymer/insertion cell,” *Journal of the Electrochemical society*, vol. 140, no. 6, pp. 1526–1533, 1993.
- [17] P. Arora, M. Doyle, and R. E. White, “Mathematical modeling of the lithium deposition overcharge reaction in lithium-ion batteries using carbon-based negative electrodes,” *Journal of The Electrochemical Society*, vol. 146, no. 10, pp. 3543–3553, 1999.
- [18] W. van Schalkwijk and B. Scrosati, *Advances in lithium-ion batteries*. Springer Science & Business Media, 2007.
- [19] J. Newman and K. E. Thomas-Alyea, *Electrochemical systems*. John Wiley & Sons, 2012.
- [20] B. Purushothaman and U. Landau, “Rapid charging of lithium-ion batteries using pulsed currents a theoretical analysis,” *Journal of The Electrochemical Society*, vol. 153, no. 3, pp. A533–A542, 2006.
- [21] H. Ge, T. Aoki, N. Ikeda, S. Suga, T. Isobe, Z. Li, Y. Tabuchi, and J. Zhang, “Investigating lithium plating in lithium-ion batteries at low temperatures using electrochemical model with nmr assisted parameterization,” *Journal of The Electrochemical Society*, vol. 164, no. 6, pp. A1050–A1060, 2017.

- [22] S. Tippmann, D. Walper, L. Balboa, B. Spier, and W. G. Bessler, “Low-temperature charging of lithium-ion cells part i: Electrochemical modeling and experimental investigation of degradation behavior,” *Journal of Power Sources*, vol. 252, pp. 305–316, 2014.
- [23] P. J. Newman, “Fortran programs for the simulation of electrochemical systems.” Accessed: 28.05.2018,
<http://www.cchem.berkeley.edu/jsngrp/fortran.html>.
- [24] M. Doyle, J. Newman, A. S. Gozdz, C. N. Schmutz, and J.-M. Tarascon, “Comparison of modeling predictions with experimental data from plastic lithium ion cells,” *Journal of the Electrochemical Society*, vol. 143, no. 6, pp. 1890–1903, 1996.
- [25] R. D. Perkins, A. V. Randall, X. Zhang, and G. L. Plett, “Controls oriented reduced order modeling of lithium deposition on overcharge,” *Journal of Power Sources*, vol. 209, pp. 318–325, 2012.

